Naval Ocean Research and Development Activity
April 1990 Report 244

Seasonal Optical Properties Derived from Coastal Zone Color Scanner Satellite Data Along the Somali Coast and the Gulf of Aden

R. A. Oriol
Planning Systems, Incorporated
Slidell, Louisiana

R. A. Arnone
Mapping, Charting, and Geodesy Division
Ocean Science Directorate

Foreword

Our understanding of the ocean environment within which the Navy operates has increased significantly in the last decade. During this time, remote sensing of the oceans from spaceborne platforms has dramatically enhanced our capability to specify vital ocean environmental parameters on a global scale. Satellite oceanography has thus been viewed with increased optimism in filling data voids in oceanography.

Satellite measurements of the optical properties (diffuse attenuation coefficient) by the Nimbus-7 Coastal Zone Color Scanner have been the focus of considerable research in defining the spatial and temporal variability for establishing the ocean optical climate. The global optical properties retrieved from the Nimbus-7 Coastal Zone Color Scanner in some instances have an accuracy of 90% with data collected in the field. Further validation of the absolute accuracy is under evaluation.

The Naval Ocean Research and Development Activity is developing an optical properties data base from Nimbus-7 Coastal Zone Color Scanner data to be used in planning naval survey operations for the Airborne Bathymetry System. This report deals with the processing and analysis of these ocean color images to derive absolute diffuse attenuation properties of the water. Images in this report represent a regional subset of a high-resolution (1 km) data base off the Somali coast. Particular attention is focused on understanding seasonal optical climatology as it is associated with supporting environmental parameters, such as satellite-derived sea surface temperature and meteorological data.

W. B. Moseley
Technical Director

J. B. Tupaz, Captain, USN
Commanding Officer

Executive Summary

Optical water properties of the world's oceans can be obtained from data collected with the Coastal Zone Color Scanner (CZCS) aboard Nimbus-7. Our understanding of the spatial and temporal variability of surface optical properties is greatly improved by synoptic images from visible channel satellites. Current satellite data processing techniques can eliminate the atmospheric contamination that contributes 90% of the visible channel signal. The remaining signal, which constitutes the ocean color, is directly related to the diffuse attenuation coefficient (K) at 490 nanometers for the upper surface waters. Calculation and geographic registration of K can be performed on each 825-m^2 image pixel of the CZCS data, and results show that the accuracy is within 92% of ship measurements.

Regional coastal optical atlases are required for planning bathymetric surveys using the Airborne Bathymetric System. CZCS data provide a method of deriving temporal and spatial variability of coastal optical properties in regions where limited ship measurements are available. This report presents a demonstration of the capability of a regional optics data base generated using CZCS data.

A series of CZCS images of the eastern Somali coast and the Gulf of Aden has been processed for the diffuse attenuation coefficient and have been used to define a regional optical data base. This data base exists in digital image form and clearly defines optical variability in response to continental winds, monsoon winds, and coastal upwelling.

This report represents an initial effort toward generating a regional atlas and demonstrates the methodology to process CZCS data for producing an optical atlas. The procedures for processing, the time requirements, the data handling, and the image file processing are presently being refined and improved based on the procedures used in this regional atlas. This atlas is the initial product produced for the Coastal Optics Planner and is intended as a subset to a global product being generated. Future regional atlases will be produced by the Naval Oceanographic Office in a manner similar to the method shown here.

Acknowledgments

Appreciation is extended to Jim Mueller and personnel of the recently closed Scripps Visibility Laboratory in La Jolla, California, for access to their CZCS data archives. Additionally, the technical assistance of Susan Walsh of the Rosenstiel School of Marine and Atmospheric Sciences, University of Miami, is acknowledged. Finally, gratitude for assistance with image processing is extended to Helen Beresford and preparation of the text to Kim Schaefer and Karla Woodall, all of Planning Systems Incorporated, Slidell, Louisiana.

This work was conducted as part of NORDA's "Coastal Optics Planner" program and was funded by Oceanographer of Navy, CNO OP-096, Program Element 63704N, as part of the Coastal Hydrographic Techniques Program.

Contents

Seasonal Optical Properties Derived from Coastal Zone Color Scanner Satellite Data Along the Somali Coast and the Gulf of Aden

I. Introduction

Historically, the oceanographic data base of optical properties is severely limited by both the number of observations and the type of measurement. The existing diffuse attenuation coefficient data base for large ocean and coastal regions is inadequate for determining spatial and temporal variability (Arnone, 1983). This data base, which resides at the National Ocean Data Center, assimilates optics data as Secchi depth measurements and contains approximately 96,000 readings that date to the early 1900s. Problems with the quality and the frequency of measurements have demonstrated that improved techniques for measuring and monitoring optical properties were warranted.

The necessity for an improved data base for monitoring the ocean optical properties is based on the requirement for electro-optical systems to operate within the ocean environment. These systems, which operate based on the propagation of visible radiation through seawater, are critically influenced by spectral optical characteristics. The Airborne Bathymetric System (ABS), under development by the Defense Mapping Agency and the Chief of Naval Operations (CNO OP-096), uses laser and multispectral scanning remote sensing systems to determine bathymetry.

This system performance is partially controlled by optical properties in coastal areas. Planning operations of ABS will be governed by understanding the coastal optical environment. Since coastal waters have extremely high spatial and temporal variability, methods to improve on data collection and analyses were required.

Ocean color imagery were gathered by the Coastal Zone Color Scanner (CZCS), aboard the Nimbus-7 satellite from November 1978 to June 1986 (Table 1). The imagery were used to determine the diffuse attenuation coefficient in the surface layer (first attenuation length). The absolute water-leaving spectral radiance in two of the CZCS channels was empirically related to the attenuation coefficient. The application of

Table 1. CZCS sensor specifications.

Channel	Center Wavelength	Bandwidth	S/N at Radiative Input (mW cm^{-2} Sr^{-1} m^{-1})	Purpose
1	443 nm	± 10 nm	>150 at 5.41	Chlorophyll Absorption
2	520 nm	± 10 nm	>140 at 3.50	Chlorophyll Correlation
3	550 nm	± 10 nm	>125 at 2.86	Hinge Point
4	670 nm	± 10 nm	>100 at 1.34	Atmospheric Correlation
5	750 nm	± 50 nm	>100 at 10.8	Land Mask
6	11.5 m	± 1 m	*$NE\Delta T$ = 0.22 K at 270 K	Surface Temperature

IFOV at nadir	0.865 m Rad. (0.05°)
Pixel size at nadir	825 m
Coregistration at nadir	>0.15 m Rad.
Swath width	1566 km
Useful nadir angles	± 39.3°
Along-track tilt	± 20°
Power requirement	11.4 W
Data rate	800 kbytes
Max. tape record time	9.5 min

*Noise Equivalent Delta Temperature

CZCS imagery in providing the optical data base allows a unique capability in determining the spatial and temporal variability. The synoptic coverage of the 1500-nmi swath of the satellite, coupled with the near-daily coverage, permits absolute optical values to be computed for each pixel within the scene. The pixel resolution represents 825 m^2 at the equator. Satellite retrieval of oceanographic data is far more cost effective than ship-gathered data, and is not limited by political boundaries (Arnone and Oriol, 1985).

The objective of this optical atlas is to assess the variability of the ocean optical properties for a small regional area at different times of the year. The area is inclusive of the Gulf of Aden and the northeastern Somali coast, and is used as additional input to the Coastal Optics Planner and in the general planning of operations.

Forty CZCS images were used in this study. The data were Level 1B data obtained from the Scripps Institution of Oceanography at La Jolla, California. Level 1B data are Nimbus-7 CZCS data that are not corrected for atmospheric contamination or navigation distortions caused by sensor optics. Data from December 1978 to January 1981 were reviewed, and an average of two cloud-free scenes per month was selected for processing.

II. CZCS Data Processing Procedures

CZCS image processing at NORDA is done using the Rosenstiel School of Marine and Atmospheric Science Display (DSP) system, and the NORDA Interactive Digital Satellite Image Processing System (IDSIPS). Uncalibrated and ungeometrically corrected (Level 1B) CZCS data were stored on computer compatible tapes (CCT) at 6250 bpi. Generally, two image files were ingested to cover the area of interest. The Ingest step is run from a user account that transfers satellite data from the source tape to a standard image file.

After Ingest with the creation of a CZCS image file, the navigation data (satellite roll, pitch, and yaw) are refined so that the optimum earth registration can be obtained. The navigation refinement is a user-interactive exercise in which the CZCS image is displayed on the monitor, and a coastal outline relative to the satellite scene displayed is written into graphics overlaying the image. This coastline is derived from the roll, pitch, and yaw data available from the original CCT. Generally the coast is only a few pixels off in alignment with the satellite image, and the user refines the alignment by interactively shifting the graphics. The shift applied to the graphics is translated into a modification to the roll, pitch, and yaw. The modifications are rewritten into the header of the image file and carried through for later processing.

After the navigation data are modified and rewritten to the image file header, the CZCS data are processed to remove atmospheric contamination. CZCS processing to obtain chlorophyll (*CHL*), diffuse attenuation length ($K490$, at 490 nanometers (nm)), normalized water-leaving radiance ($nLw443$, $nLw520$, $nLw550$), and aerosol radiance ($La670$) is performed in a series of interrelated steps. Normalized water-leaving radiance is the radiance that leaves the ocean surface, assuming that solar zenith is directly overhead. It is determined by viewing as if the detector were positioned just above the surface and directed vertically downward (independent of scan angle).

Obtaining quantitative ocean parameters (*CHL* concentration, attenuation coefficients) from CZCS data requires accurate water-leaving radiance (at 443, 520, and 550 nm) retrievals. *CHL* concentrations are calculated with a three-channel algorithm using water-leaving radiances at 443, 520, and 550 nm (Gordon and Clark, 1980). Methods to determine normalized water-leaving radiance are based on the algorithm presented in Gordon et al. (1985), and are based on a linear combination of the total radiance sensed at the satellite into atmospheric Rayleigh radiance, atmospheric aerosol radiance, and water-leaving radiance.

Two atmospheric Rayleigh scattering models which are part of the processing procedure can be applied to the CZCS data: a single scattering model valid for calculations within 55° of the solar equator, and a multiple scattering polarization model that extends quantitative calculations to within 65°. The Rayleigh radiance is computed from geometrical considerations of solar and spacecraft altitudes and subtracted from the total radiance for each of the channels. Rayleigh radiance contribution represents about 70–80% of the total signal.

Atmospheric aerosol radiance (large particle scattering) is calculated by assuming the 670-nm channel is representative solely of aerosol contribution and there is no water-leaving radiance at this wavelength. The aerosol radiance contribution in the 443-nm, 520-nm, and 550-nm channel is corrected by a weighted subtraction of the 670-nm channel. The weight of the subtraction, termed the "epsilon coefficients" (atmospheric correction coefficients), is initially set at $E = 1.0$. More accurate epsilons are determined for each specific image using the clear water-radiance method (Gordon and Clark, 1980). This method is based on interactive selection of low chlorophyll regions within the scene, i.e., $CHL < 0.25$ mg/m^3.

Following initial processing with $E = 1$, four images (i.e., calculated chlorophyll ($nLw(443) : nLw(550)$), atmospheric aerosol radiance ($La(670)$) and normalized water-leaving radiance at $Lw(550)$ and $Lw(520)$ are simultaneously displayed on the monitor for selecting more accurate E coefficients for the 443-nm, 520-nm,

and 550-nm wavelengths (DSP function, CALEPS routine calculate E). Low-chlorophyll areas are selected in regions of minor to moderate aerosols ($La670$). The CALEPS routine uses the low-chlorophyll concentrations and calculates coefficients from a 5 × 5 pixel box centered at the sample and returns values of aerosol radiance, atmospheric Rayleigh-removed radiance, standard deviation of sensor counts, and normalized water-leaving radiance. Criteria have been established for each of these values for reliable epsilon determination. These criteria are designed to eliminate problems with in-water scattering, sun glint, cloud, scan-edge effects, low $La670$, no clear water, etc. Valid epsilons are selected, based on

- $nLw(550)$ approximately 0.3 mW/cm^2 · μm · Sr chlorophyll area with little to no in-water scattering);
- $0.3 < La670 < 1.0$ (above or below this threshold indicates a high scan angle or the effects of sun glint);
- $0.9 < E_{550} < 1.2$ (values outside these limits indicate problems with in-water scattering, sun glint, clouds, scan edge effects, low $La670$, no clear water);
- $nLw(520) = 0.5 \pm 0.05$ (a larger difference indicates the possible presence of in-water scatterers).

A repetitive interactive process is performed until acceptable epsilons are determined. Upon exiting CALEPS, the selected E coefficients are added to a data base for later review and for use in the final processing.

The removal of the atmospheric contributions of Rayleigh and aerosol scattering leaves the resulting water-leaving radiances in three channels—443, 520, and 550 nm. Empirical relationships have associated these spectral water-leaving radiances with the *CHL* concentrations and the diffuse attenuation coefficient. Gordon and Clark (1980) have developed a branching algorithm using the three water-leaving radiances for *CHL*.

$$CHL = \left(\frac{Lw(443)}{Lw(550)}\right)^{-1.269} - 0.297, \quad (1)$$

where $CHL < 1.0\,\text{mg/m}^3$, and

$$CHL = \left(\frac{Lw(520)}{Lw(550)}\right)^{-3.975} - 0.074, \quad (2)$$

where $CHL > 1.0\,\text{mg/m}^3$, and $Lw(443)$, $Lw(520)$, and $Lw(550)$ are the water-leaving radiances at 443, 520, and 550 nm. The diffuse attenuation coefficient at 490 nm was determined by an empirical relation of the water-leaving radiance of 443 and 550 nm (Austin and Petzold, 1980).

$$K(490) = (0.0883 \left(\frac{Lw(443)}{Lw(550)}\right)^{-1.491}) + 0.022 \quad (3)$$

The final phase reprocesses the CZCS image for newly selected E coefficients and puts the image into a Mercator map projection. The atmospheric correction step computes a 6-channel output file consisting of the following data sets

File 1. $nLw(443)$
File 2. $nLw(520)$
File 3. $nLw(550)$
File 4. $(La670)$
File 5. $(K490)$
File 6. *CHL*

This 6-channel image output is passed to the DSP Remap step (Remap transforms the image from satellite scan coordinates to a specified standard map projection). For this study, the CZCS imagery were remapped into a 1024 × 1024-pixel Mercator projection. The upper-left corner was selected as 15°N, 45°E, extending 10.24° to the east and the south of this point; each pixel represents 0.6 nautical miles (nmi) and maintains, as closely as possible, the satellite resolution. If available, coincident thermal CZCS data were also processed from the level 1 tape passed to Remap. After completing the Remap routine, the earth-registered CZCS data are displayed on the IDSIPS monitor for a quality control check.

During the quality control check the image is displayed and reviewed for three points. First, the coastline corresponding to this exact projection is generated from the Central Intelligence Agency data base and is compared with the results of the Remapped CZCS image. If the coastline alignment is not satisfactory, then the Remapped output is rejected, and the original Ingest file is renavigated and remapped. The second point evaluates the computed chlorophyll concentrations in low-chlorophyll regions. The image is displayed with a color table by which the user can identify regions that are overcorrected or undercorrected as a result of the selected E coefficients. If rejected, the E coefficients are recalculated, and the image is remapped. The third review point evaluates the total cloud coverage. In many instances, the percentage of clouds in an area and their location within the area are difficult to determine until the image is remapped and reviewed. If too many clouds occur over the area of interest or if the clouds cover a key point in the scene so that further analysis is useless, then the image is rejected. Remapped imagery that pass this three-point evaluation are archived on 9-track tape and are transferred to a separate disk pack that can be retrieved without the time spent required for tape input and output.

The file nomenclature uses a 10-character alphanumeric string to identify each archived file. The nomenclature specifies a three-character designator for

the month, followed by a two-digit designator for the day of the month and a four-character designator to specify the data set.

APR11_N520 is the nomenclature for the April 11 normalized, water-leaving radiance at the 520-nm wavelength. The first six characters for each of the other output files for this day are identical but their ending characters vary, i.e., N443, N550, L670, CHLOR, K490 and, when available, infrared (IR).

III. Results

Figure 1 shows the area selected for processing. For this region, a 1-km data base has been established from the CZCS imagery for inclusion into the Coastal Optics Planner. Table 2 lists the individual CZCS scenes used in this study. The data set starts in December 1978 and extends through January 1981. Two cloud-free images were selected for each month to examine the seasonal and interannual variability. Table 2 also presents the epsilon values used in processing these individual scenes. Note that the summer months have lower epsilons than other seasons.

The color scheme shown in Figure 2 is used for all the CZCS images processed in this report and represents the phytoplankton concentrations and corresponding diffuse attenuation coefficient. All the images presented here are derived chlorophyll-pigment image files; however, all six channels are available in the data base. The diffuse attenuation coefficient, $K(490)$, can be calculated from the chlorophyll-pigment concentration (Austin and Petzold, 1980) by the following equation.

$$K(490) = 0.119\ [CHL]^{1.122} + 0.022 \qquad (4)$$

The general oceanography in the region is defined by the variability of the Somali Current and the influence this current has on the shelf and coastal dynamics. Typically, the Somali Current changes significantly in response to the onset of the southwest (summer) and northeast (winter) monsoon season. As these climatic changes occur, rapid transitions observed in the Somali Current are coincident with the wind-reversal pattern associated with the high- and low-pressure systems that create the monsoon flow. Oceanic circulation patterns change substantially in the region (see Fig. 3) during the monsoon season (Deutsches Hydrophisches Institute, 1960).

The monsoon is a seasonal wind that blows from continental interiors (or large land areas) to the ocean in the winter and in the opposite direction during the summer. The monsoons blow from the northeast during January and from the southwest in July. In winter the winds result from the high-pressure area situated over Siberia. In the summer the winds result from the low-pressure area over central Asia. The summer monsoon winds contain excessive precipitation. The winter monsoons typically have clear skies.

In May, a northward current develops off Somali originating north of the equator from weak, southerly winds. At 5°N, the current turns eastward and produces a coastal upwelling wedge that induces cold upwelling along the coast (Schott, 1983). Coastal Ekman upwelling regimes occur to the north of the wedge. During June, the winds increase and produce an anticyclonic gyre north of 5°N. The current turns eastward at 8°–9°N and generates a second, cold, upwelling "wedge" along the coast.

Table 2. Selected CZCS images and epsilon values used in the processing channels.

Date	Orbit	443 nm	520 nm	550 nm
December 30'78	927	1.154	1.127	1.097
January 10'79	1079	1.047	1.062	1.048
January 28'79	1328	0.944	0.996	0.997
January 20'79	1646	1.025	1.047	1.037
February 27'79	1743	1.025	1.047	1.037
March 4'79	1812	1.376	1.255	1.193
May 17'79	2835	0.979	1.019	1.014
June 2'79	3056	1.185	1.145	1.111
June 30'79	3443	0.95	1.0	1.0
July 10'79	3581	0.95	1.0	1.0
July 27'79	3816	0.976	1.016	1.013
August 3'79	3913	0.959	1.006	1.005
August 13'79	4051	0.95	1.0	1.0
September 3'79	4341	0.95	1.0	1.0
September 10'79	4438	0.95	1.0	1.0
September 26'79	4659	0.95	1.0	1.0
October 3'79	4756	1.096	1.091	1.071
October 18'79	4963	1.232	1.172	1.132
October 25'79	3060	1.164	1.133	1.102
November 15'79	5350	1.286	1.204	1.156
November 21'79	5433	1.141	1.119	1.091
December 7'79	5654	1.126	1.11	1.085
December 28'79	5944	1.257	1.187	1.143
January 8'80	6096	1.096	1.091	1.070
January 24'80	6317	1.233	1.173	1.133
February 4'80	6469	1.012	1.04	1.031
February 27'80	6787	0.981	1.02	1.015
March 3'80	6856	1.259	1.183	1.144
March 21'80	7105	1.203	1.159	1.119
April 27'80	7616	1.151	1.125	1.096
May 20'80	7934	1.195	1.151	1.115
June 6'80	8169	1.135	1.115	1.088
June 10'80	8224	1.309	1.217	1.165
August 5'80	8998	1.055	1.066	1.051
August 27'80	9302	1.321	1.224	1.17
September 20'80	9634	1.037	1.055	1.043
November 7'80	10297	1.127	1.111	1.085
December 27'80	10988	1.222	1.167	1.128
January 20'81	11320	1.216	1.164	1.125
January 26'81	11403	1.005	1.035	1.027

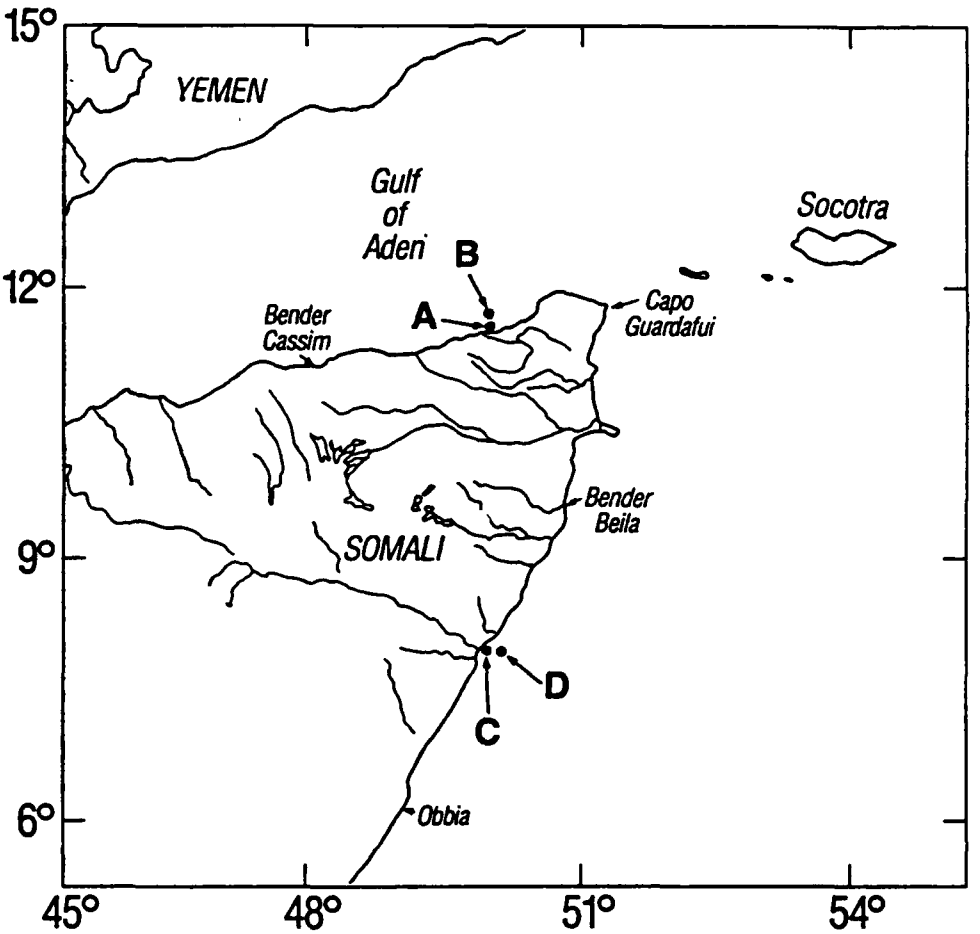

Figure 1. Map location of the Somali coast and Gulf of Aden study area. This Mercator projection of the coastline represents the 1024 × 1024-pixel area where ocean optical and thermal products were produced. Points A, B, C, and D shown in this figure correspond to locations where the optical variability is illustrated in Figure 8.

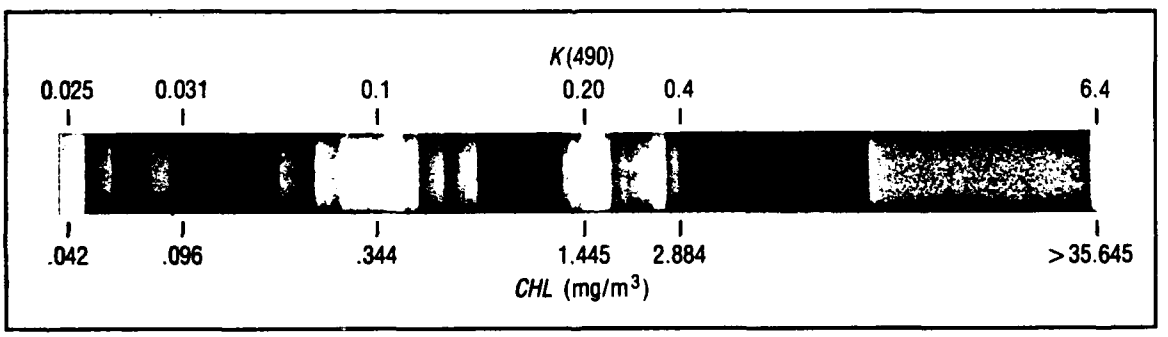

Figure 2. Color bar used in all CZCS images for the chlorophyll concentration and corresponding diffuse attenuation coefficient at 490 nm.

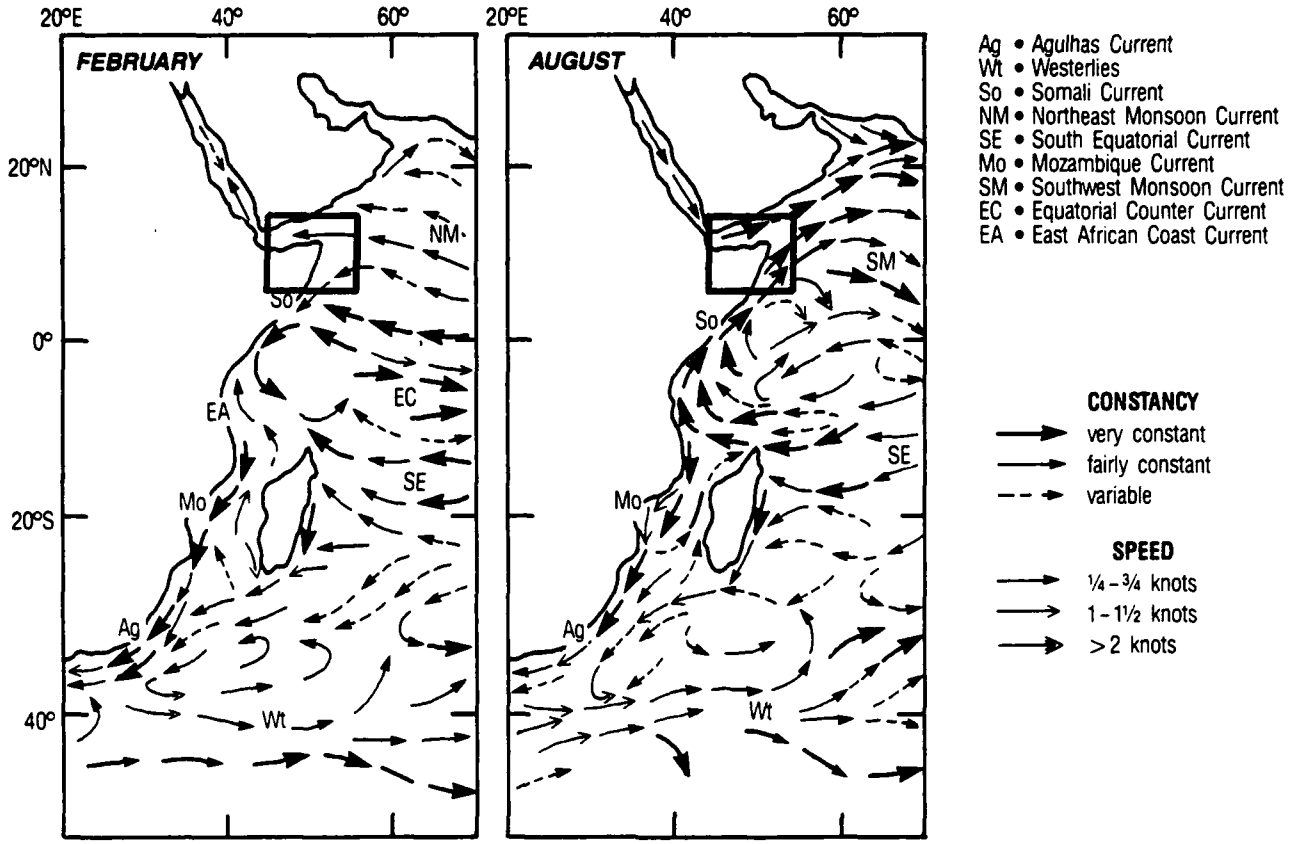

Figure 3. Contrasting circulation patterns between the monsoon seasons, Deutsches Hydrographisches Institute (1960).

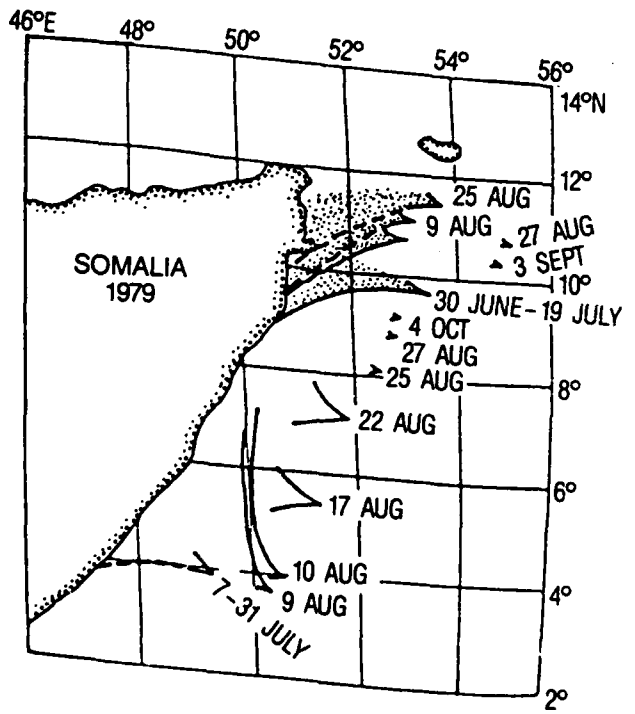

Figure 4. Schematic showing the position of the northward propagation of the upwelling wedges of eastward-flowing Somali Current at different times based on sea surface temperature imagery (from Evans and Brown, 1981).

Late in the summer (August/September), a dramatic change occurs with the southern upwelling wedge (5°N) as the wedge begins to propagate northward. This change suggests a breakdown in the gyre pattern, as well as the development of a continuous northerly boundary current off the coast from the equator to 10°N. The northward propagation of the cold wedge is observed in satellite imagery (Evans and Brown, 1981).

Schott (1983) and Evans and Brown (1981) show the evolution of the coastal current and the position of the upwelling wedge at different times of the year in 1979 (Fig. 4), based on the thermal IR satellite images and ship mooring data. This cold-wedge feature will be shown to have a corresponding ocean color signature of elevated chlorophyll concentration. In viewing the following sequence of CZCS satellite data, it is important to understand the oceanographic and meteorological parameters that produce and influence the bio-optical properties.

The sequence of CZCS images that comprise the data base is at a spatial resolution of 1-km and represents a 1024 × 1024-km area. Figure 5 illustrates a representative subsample (2 × 2) of images. In all the imagery the clouds and land have been masked black. The Mercator grid has been overlaid for scale. To further

illustrate the spatial resolution of the data base, a 512-km^2 image of the September 3 image (Fig. 6) is enlarged by two in Figure 7. This figure illustrates individual pixels that represent the full 1-km pixel resolution. The complex distribution of chlorophyll and the optical properties along the Somali Coast are clearly observed in this image. The spatial variability is difficult to describe, except in image format. However, the applicability of the CZCS data for describing the coastal optical climate is clearly demonstrated.

To illustrate the utility of the sequences of CZCS images for assessing the coastal optical properties, four points were selected at locations along the Somali coast. These points are shown in Figure 1:

Point	A	B	C	D
	11.51°N	11.55°N	7.82°N	7.82°N
	50.02°E	50.02°E	49.83°E	49.87°E

Points A and B, in the Gulf of Aden, represent a coastal environment (A) and offshore (B). Points C and D are similarly representative in the Somali current. The diffuse attenuation coefficients for these points are plotted in Figure 8 for the 2-year cycle when the CZCS images were processed. The trends of these plots clearly show a seasonal influence at different coastal regions.

In the Gulf of Aden the offshore (point B) location clearly shows higher diffuse attenuation coefficient in fall and winter. The inshore station (A) illustrates continuously high values with less seasonal dependence.

In the Somali coastal area, a seasonal trend is shown in point C, where higher diffuse attenuation coefficients are shown to correspond to the monsoon seasons in spring and summer. Slightly lower $K(490)$ are observed offshore (D).

The following sequence of images has been effectively subsampled by four to obtain four images on a single page. Although this resolution is poor, it will clearly be adequate for describing the interaction of the meteorological, physical, oceanographic, and bio-optical responses in the Somali coastal waters.

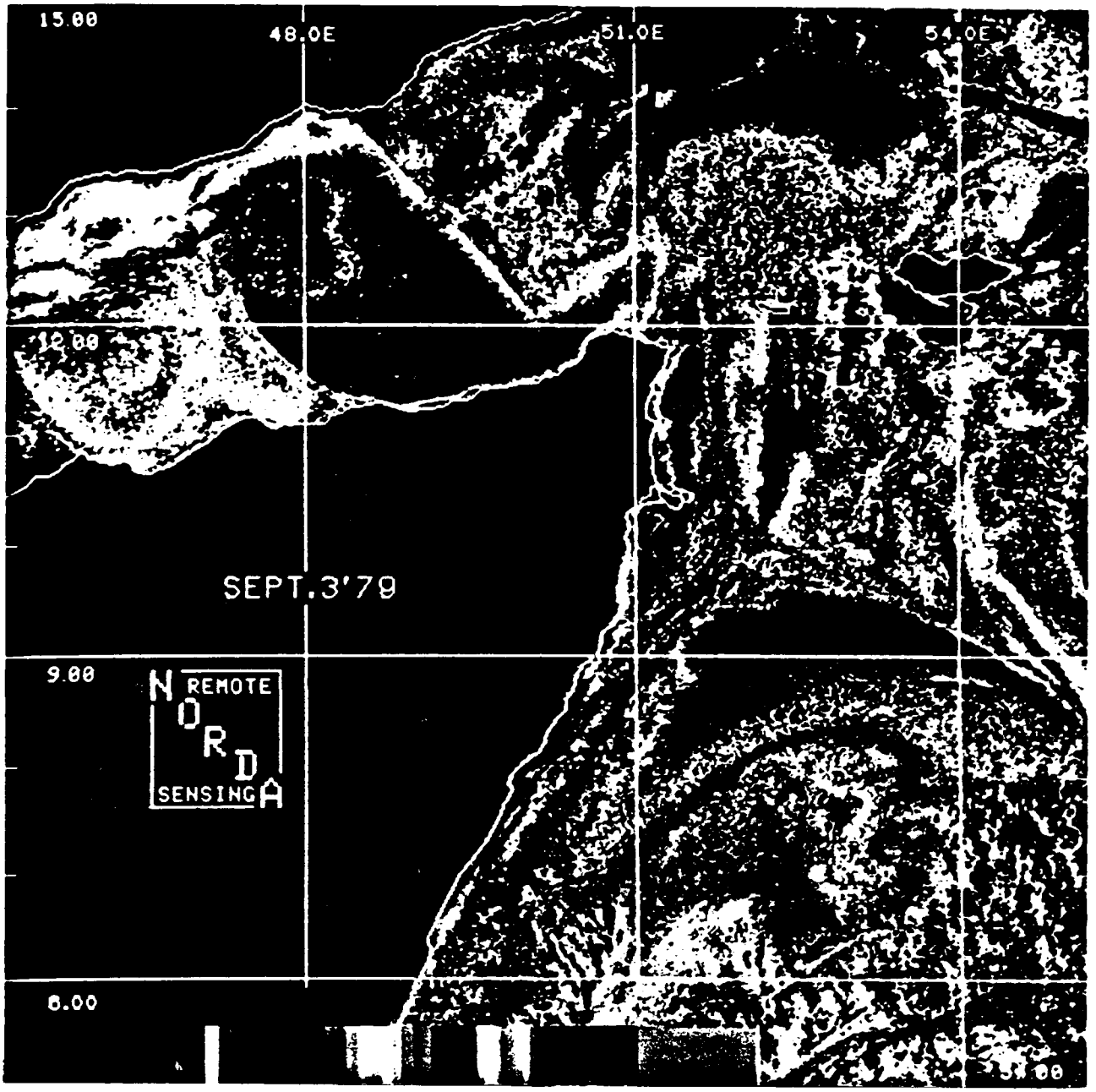

Figure 5. This CZCS image is a representative subsample (2 × 2) of the image data base from September 3, 1979.

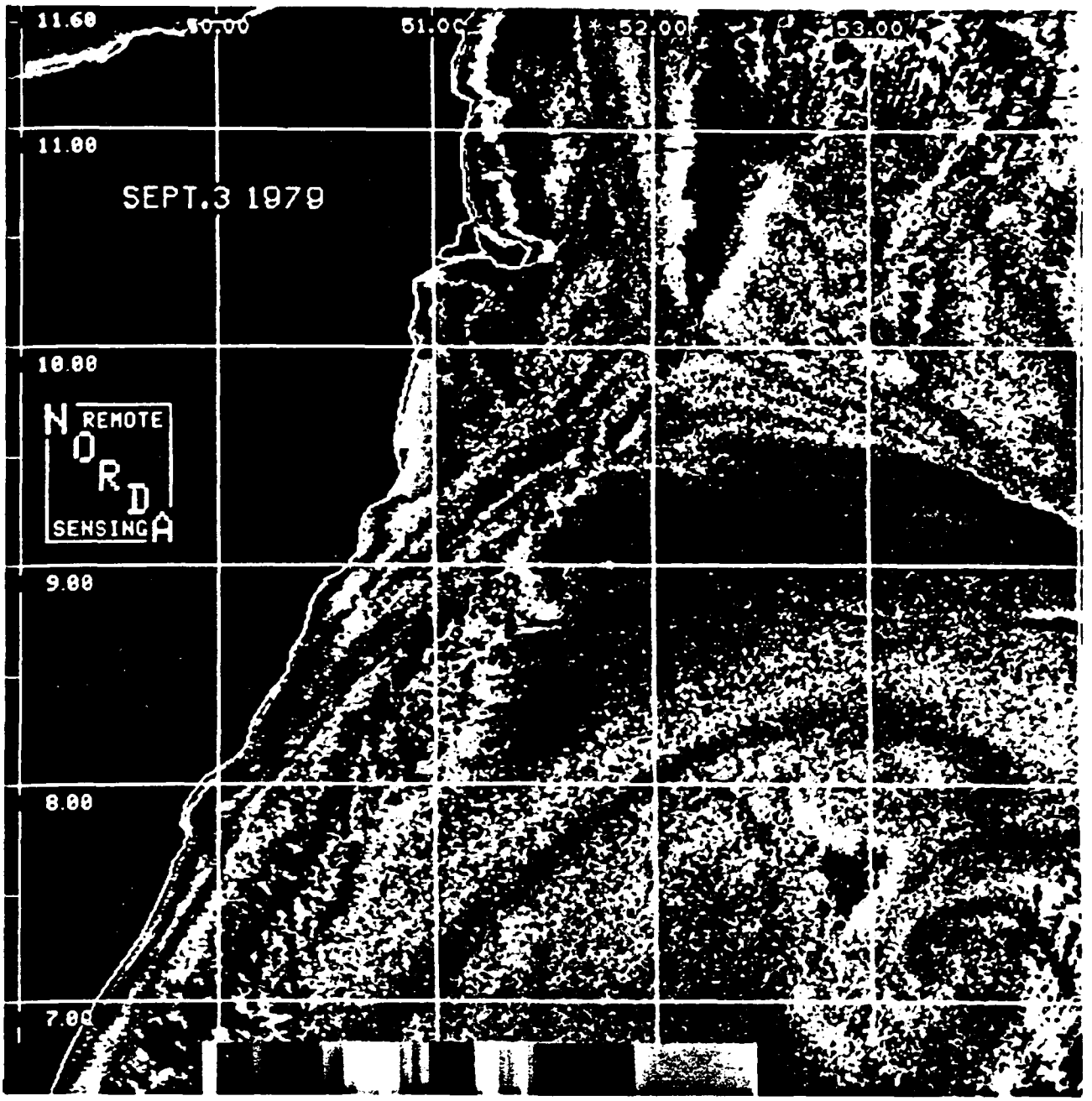

Figure 6. This CZCS image represents 512 × 512-pixel full resolution (512 km^2) of the optical data along the Somali Coast. An area four times larger than this area is included in the regional data bases.

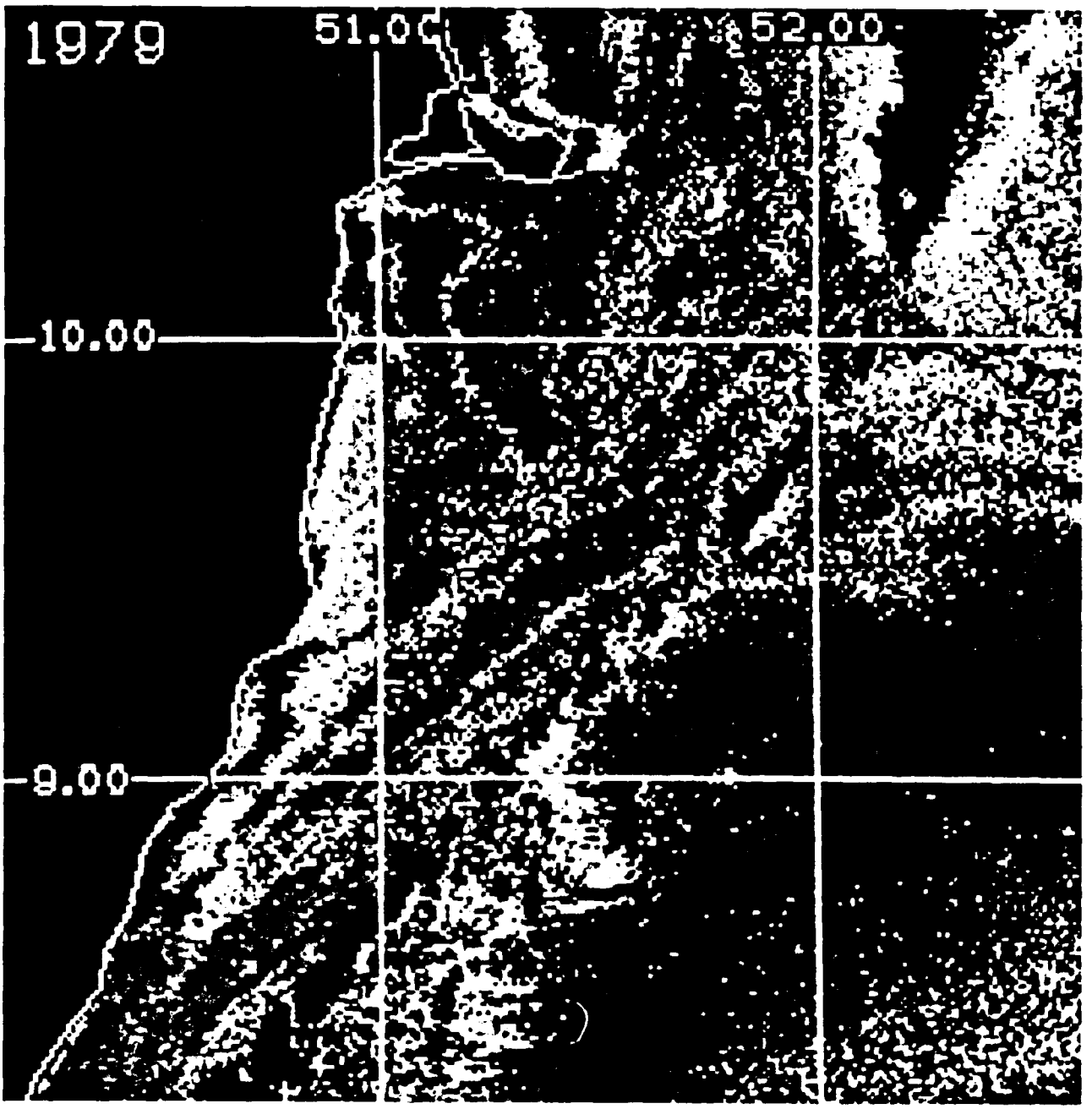

Figure 7. Enlarged section (256 km^2) of the CZCS optical properties along the Somali coast illustrates the spatial resolution of the 1-km CZCS regional data base.

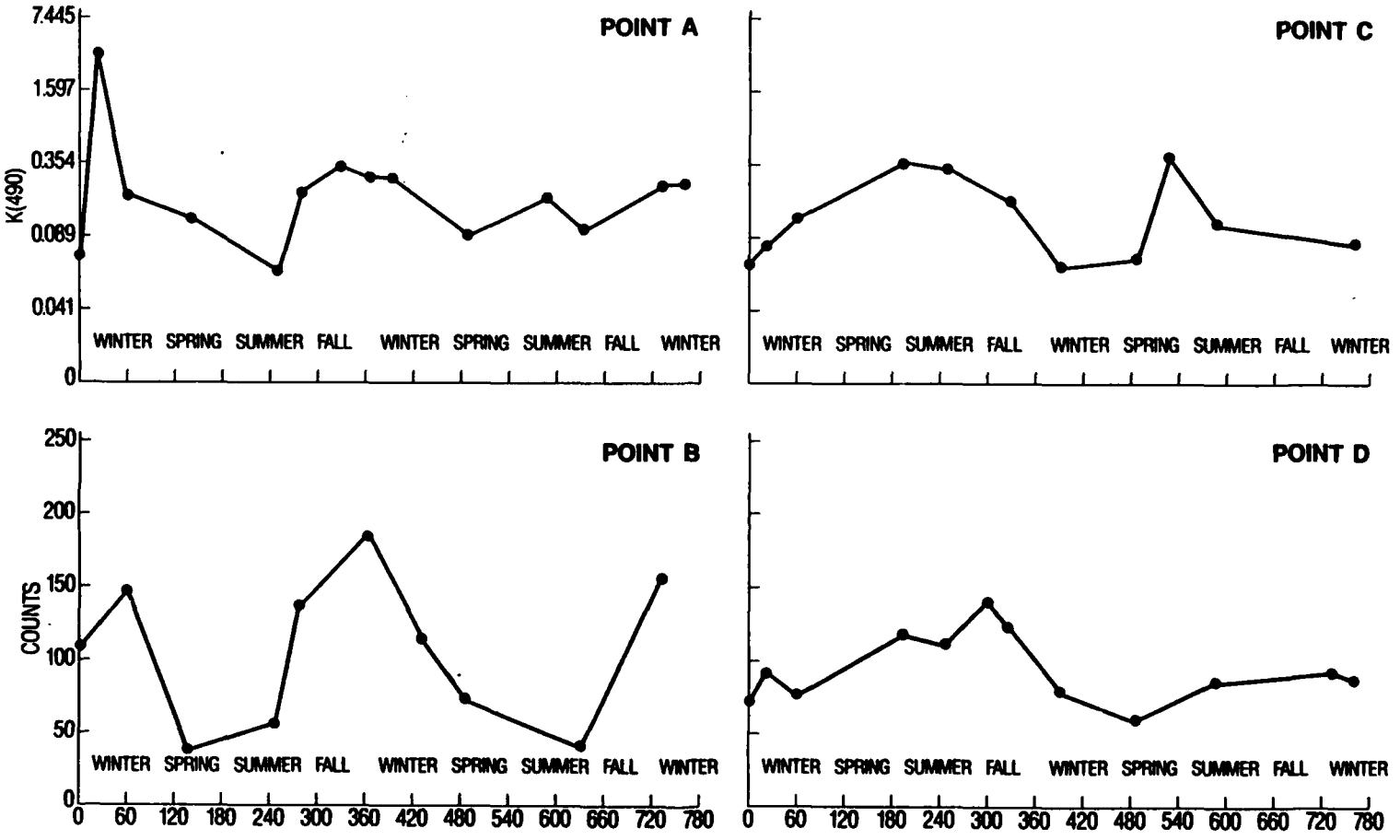

Figure 8. Seasonal distribution from selected points A–D (Fig. 1) from the 2-year sequence illustrates the variability of the diffuse attenuation coefficients, K(490). The monsoon season (spring and summer) shows increased optical attenuation.

December 30'78, January 10'79, and January 28'79

This period of satellite imagery (Fig. 9) shows the Somali coast and the southern Saudi Arabian coast to the left and the top of the scene. Scattered clouds (black) are observed throughout the images. The general chlorophyll concentration and the optical properties during this period are comparatively low, ranging between 0.05 and 0.30 mg/m^3 ($K(490)$ = 0.026 to 0.1 m^{-1}). Two small eddies are observed in the December 30 image. The first eddy, located southwest of Socotra Island, extends 100 km offshore, and has an elevated chlorophyll concentration near 0.89 mg/m^3 ($K(490)$ = 0.1 m^{-1}). The second anticyclonic west-northwest eddy, located in the Gulf of Aden, is approximately 150 km in diameter and has reduced pigment concentrations of 0.22 mg/m^3 ($K(490)$ = 0.044 m^{-1}). Evans and Brown (1981) indicate that mean sea surface temperatures during this time are at a minimum within the waters between 12°N and 6°N and range from 25.5°C to 26.64°C. The monsoon flow is from the northeast (winter monsoon). Wind contours over the eddies indicate wind speeds between 5.1 and 10.3 m/sec. The cooler, drier, continental air is well established over the area during this time, and satellite images of the ocean are clearer.

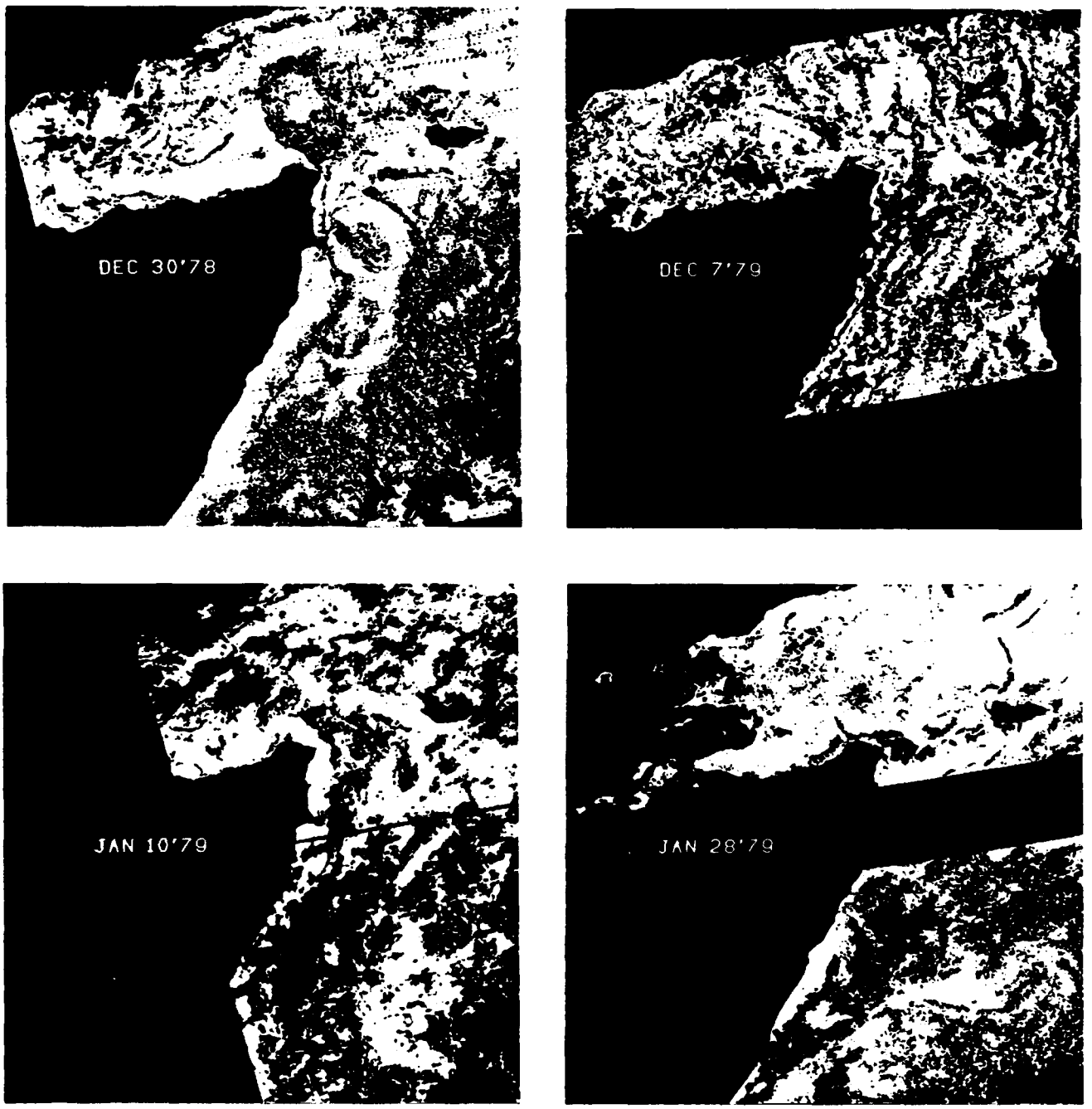

Figure 9. December 30'78, December 7'79, January 10'79, and January 28'79 image sequence.

February 20'79, February 27'79, and March 4'79

A slight increase in the chlorophyll concentration is observed in February (Fig. 10). February 20 shows a northward-moving, chlorophyll-poor (<0.02 mg/m^3, $K(490) = 0.023$ m^{-1}) Somali current propagating northward off the coast. A large meander at 8°N shows an offshore extension of the current. Notice that this region of 0.02 mg/m^3 ($K(490) = 0.023$ m^{-1}) extends to the coast and that it is not present in the February 27 image. Circulation patterns showing the Somali current in this sequence are better defined. All three scenes indicate the region in the Gulf of Aden within 5 km of the Somali coast as a region of slightly higher chlorophyll levels ($CHL = 2.3-2.8$ mg/m^3, $K(490) = 0.3-0.4$ m^{-1}). The Gulf of Aden circulation is illustrated as a complex mixture of eddies and high horizontal chlorophyll variability. Within the flow, chlorophyll concentrations are generally moving from south to north between 6°N and 12°N, and are on the order of 0.07 mg/m^3 ($K(490) = 0.028$ m^{-1}). By March 4, the offshore chlorophyll concentrations have diminished (purple to white), but the coastal conditions remain the same. A remnant of the meander shown on February 20 at 8°N is present on March 4. During this period, wind speeds from the northeast are relatively stable at 10.3 m/sec, suggesting minimal upwelling in the coastal regions. Additionally, data from hydrographic casts also indicate an absence of upwelling during this season. Mean sea surface temperatures range from 25.5°C to 26.6°C (La Violette and Frontenac, 1967). No imagery were available for the area during late March or April 1979.

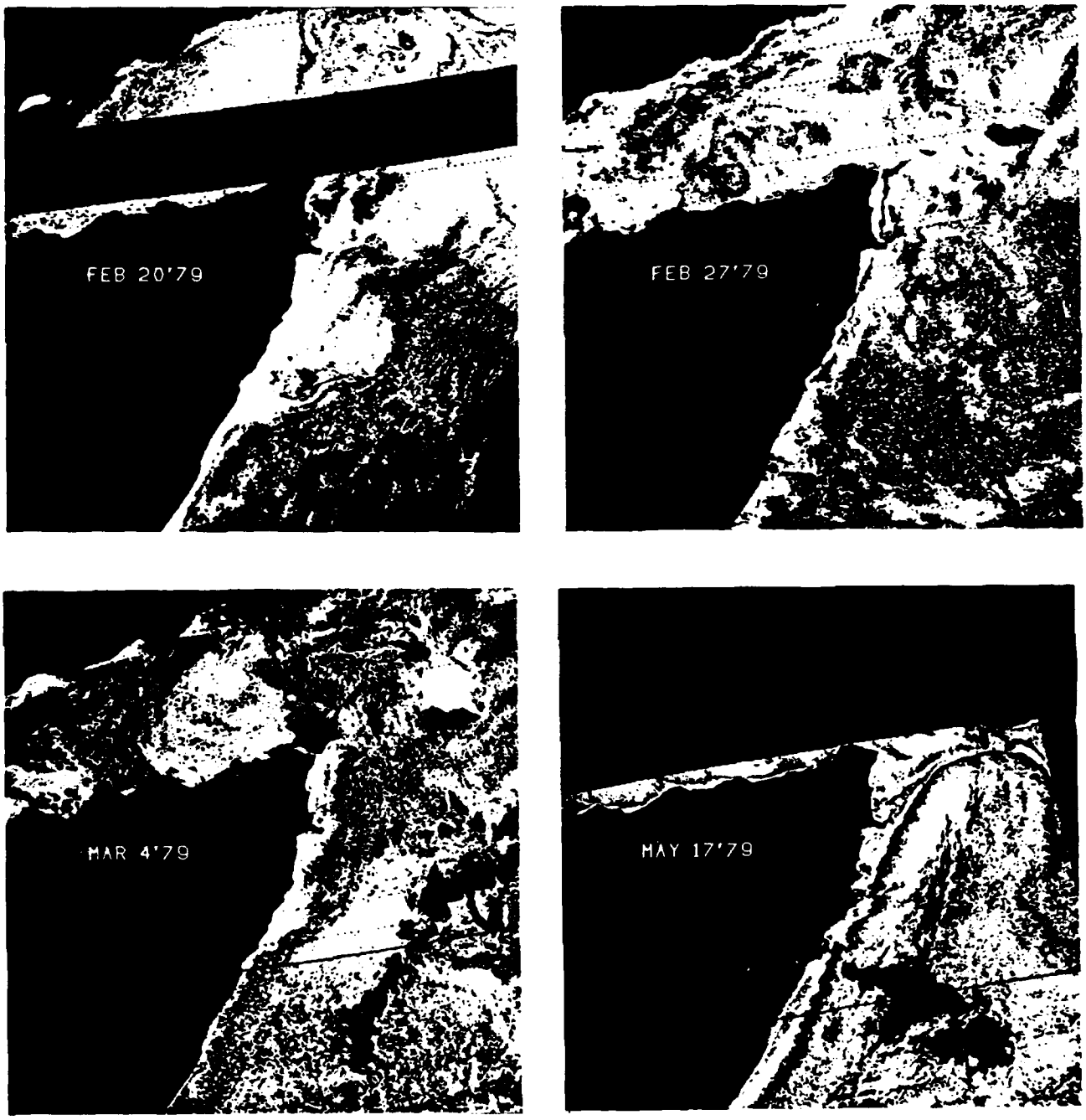

Figure 10. February 20'79, February 27'79, March 4'79, and May 17'79 image sequence.

May 17'79, June 2'79, June 30'79, July 10'79, and July 27'79

During this period (Figs. 10 and 11) the area began to be affected by the onset of the summer monsoon season, and satellite analysis is contaminated by cloud cover. By mid-May, coastal waters between 2°N and 7°N begin to cool, and a weak front develops between 7°N and 10°N (Brown and Evans, 1981). The thermal gradient in the southern frontal region was 0.02°C/km, and temperatures along the coast of Somali varied between 28°C and 26°C. Gradients in the northern region (8°N to 10°N) were weak, and the average temperature was still around 30°C in the northern region (Brown and Evans, 1981). The May 17 image indicates that the Somali current extends offshore at 10°N and extends toward the island of Socotra. This offshore movement is farther north than previous satellite images illustrate. The offshore extension clearly reveals the upwelling wedge. The chlorophyll levels within the wedge are 0.1 mg/m^3 ($K(490) = 0.031\ m^{-1}$) and are the product of upwelled coastal waters. These elevated chlorophyll waters are entrained into the easterly flow and are advected offshore south of Socotra Island.

The June 2 image indicates that the easterly flow south of Socotra has changed toward the north into the Gulf of Aden. The development of a large anticyclonic eddy is observed in the Gulf. The high variability in the chlorophyll concentrations indicates that dynamic physical events are occurring during this period at 10°N.

The June and July imagery indicate that the northward flow along the Somali coast is still present and that higher concentrations of chlorophyll, which range from 0.3-2.5 mg/m^3 ($K(490) = 0.1-0.4\ m^{-1}$), are present. Notice that in late June and July, an elevated coastal chlorophyll region is present to the south at 8°N. This region is the development of second wedge feature, which results as a meander in the Somali current. The southwest (summer) monsoon is near its maximum in late June, when wind speeds approach from the southwest at 10.3-15.4 m/sec. These winds are responsible for increased upwelling and elevated chlorophyll along the Somali coast. Sea surface temperatures indicate a cooling to 26°C in this region (8°N), and a -4°C change in coastal waters. Near mid-July the southwest monsoon has reached maximum strength, and two wedges of high chlorophyll are observed at the coast: one at 10°N and the other at 8°N.

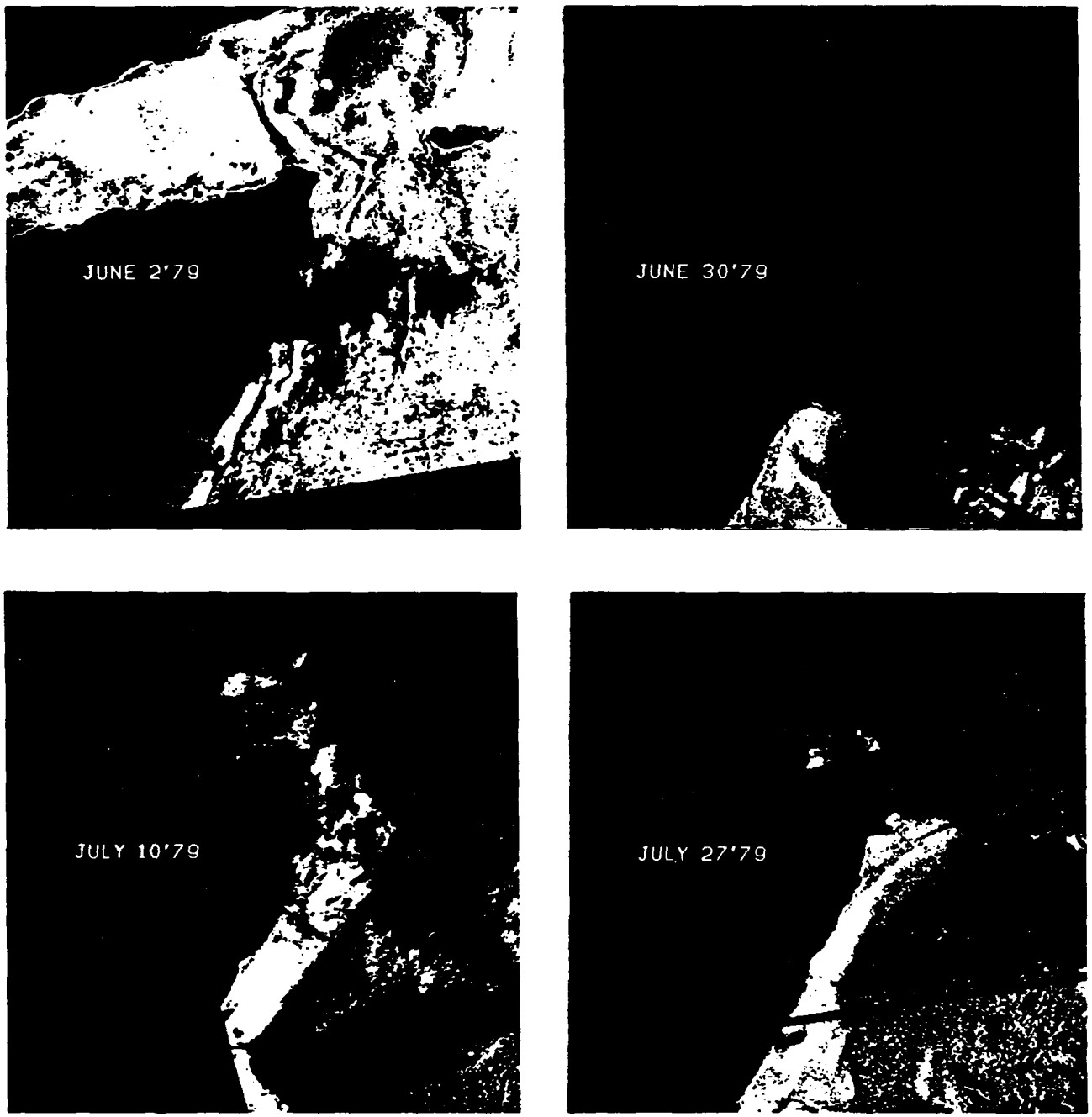

Figure 11. June 2'79, June 30'79, July 10'79, and July 27'79 image sequence.

August 3'79—October 25'1979

Eight images are used in this sequence (Figs. 12 and 13) to define the observed circulation patterns defined by the chlorophyll distributions. Chlorophyll levels are distinctively higher and occur farther offshore. The northern upwelling wedge, which occurs at 10°N, is observed to then propagate southward (August 13, September 3, and October 18). This wedge is characterized by cold water and is marked by an oxygen minimum and a nutrient maximum near the coast (75 km in diameter). The chlorophyll levels within the wedge range between 1.0 and 2.7 mg/m^3 ($K(490) = 0.1\text{-}0.4\ m^{-1}$), and indicate a sharp frontal boundary at the Somali Current that has chlorophyll levels 0.04–0.07 mg/m^3 ($K(490) = 0.025\text{-}0.028\ m^{-1}$). Historical ship drift data (Evans and Brown, 1981) show the Somali current in August, during the final phase of the summer monsoon, as an extended boundary current that flows northeastward along the East African coast from south of the equator to about 10°N, where it leaves the coast to the east. Surface temperatures during this time range from 26°C offshore to less than 18°C in the upwelling areas north of where the Somali Current veers offshore.

In the Gulf of Aden, an anticyclonic ring (75 km in diameter) is clearly defined in the September 26 and October 3 imagery, which show high chlorophyll levels of 0.096 mg/m^3 ($K(490) = 0.031\ m^{-1}$). A second, much smaller (50 km in diameter) cyclonic eddy with lower chlorophyll concentration is evident during the September 26, October 3, and October 18 sequence. The movements of these eddies during this time indicate complex dynamics in the Gulf, which is representative of strong variability in the chlorophyll concentrations. These offshore physical events do produce changes in the coastal optical and chlorophyll concentrations.

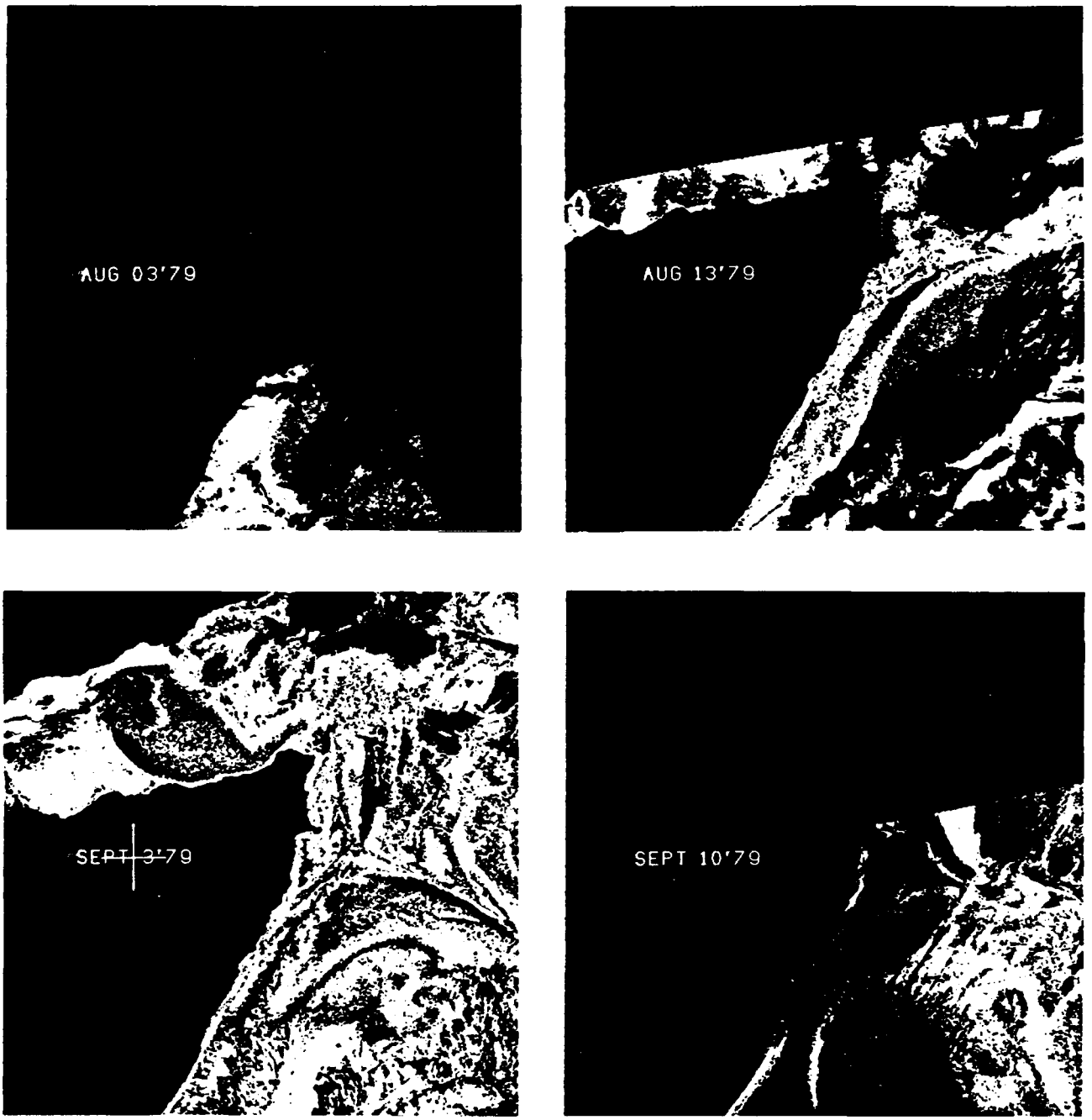

Figure 12. August 3'79, August 13'79, September 3'79, and September 10'79 image sequence.

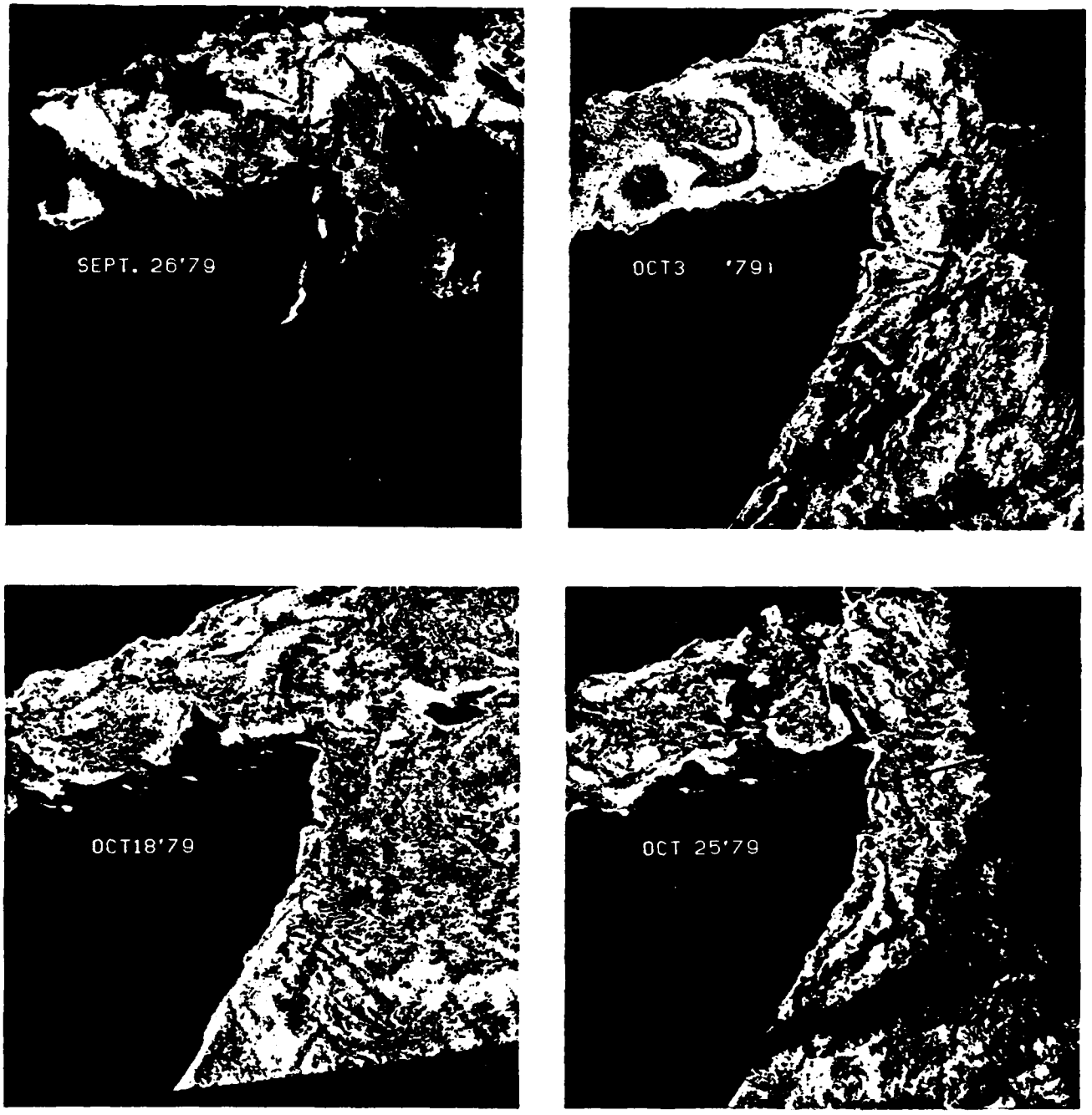

Figure 13. September 26'79, October 18'79, and October 25'79 image sequence.

November 15'79, November 21'79, and December 28'79

The highest chlorophyll concentrations were observed on November 21 and contained concentrations on the order of 1.445–2.884 mg/m^3 (K(490) = 0.2–0.4 m^{-1}). The positions of the Somali current and the wedge are observed at 7.5°N in this image (Fig. 14). Coastal optical properties indicate high variability. The chlorophyll levels decrease on December 28 to values of 0.20–0.344 mg/m^3 (K(490) = 0.042–0.1 m^{-1}).

During this period the region is undergoing a transition from the southwest (summer) monsoon season to the northeast (winter) monsoon season. The cooler coastal upwelling is lessening, and the coastal and offshore sea surface temperatures are increasing from 25.5°C to 27.2°C in September and November.

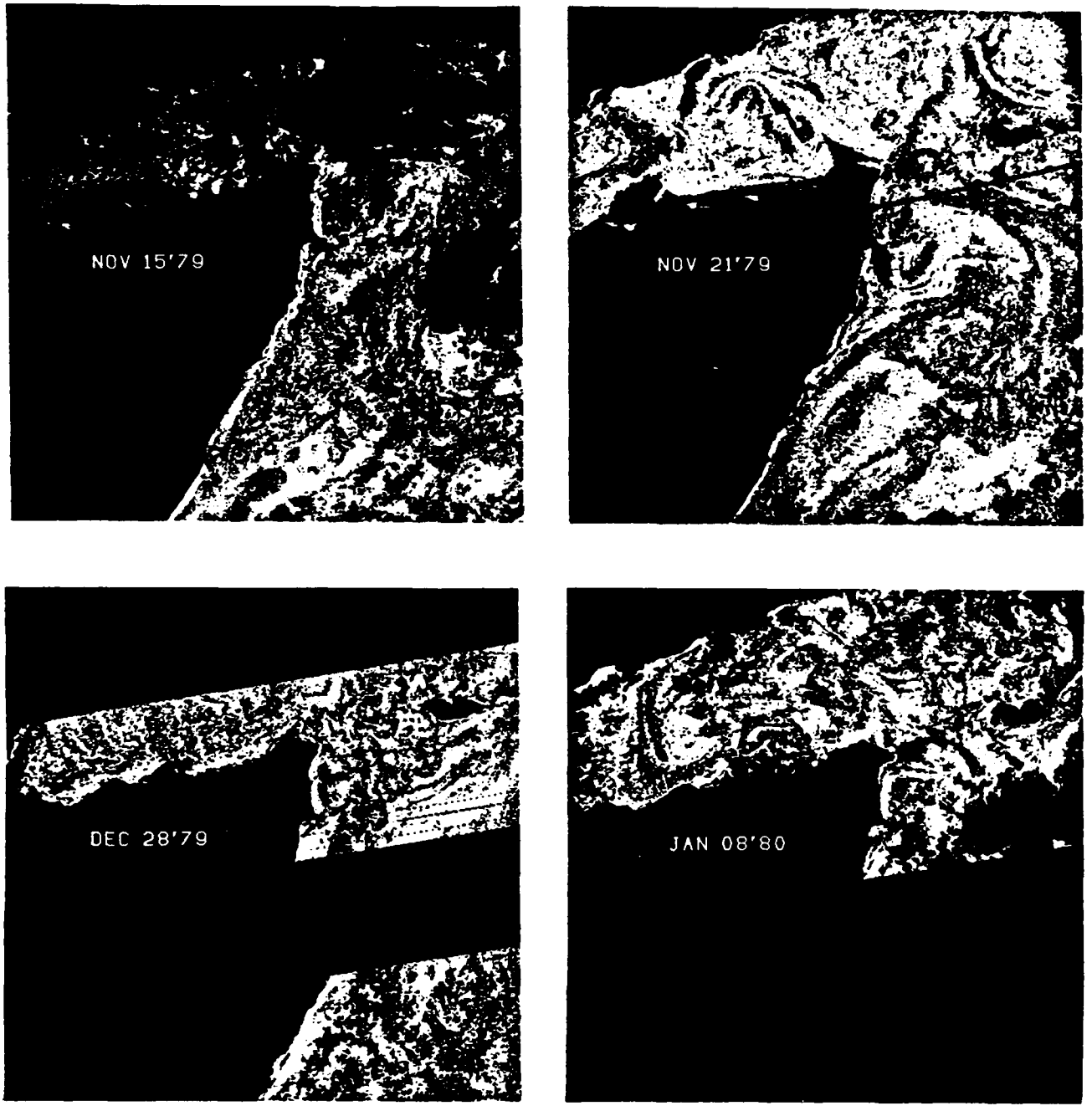

Figure 14. November 15'79, November 21'79, December 28'79, and January 8'80 image sequence.

January 8'80, January 24'80, February 4'80, February 27'80, and March 3'80

Chlorophyll concentrations similar to those shown earlier for 1979 are shown in this sequence (Figs. 14 and 15). Relatively lower chlorophyll concentrations are observed during this period. The offshore flow east of Somali is not well defined. Chlorophyll concentrations are low. The range from 0.096 to 0.38 mg/m^3 ($K(490)$ = 0.031–0.1 m^{-1}) along the Somali coast results from a decrease of coastal upwelling. In the Gulf of Aden, chlorophyll concentrations are substantially higher, ranging from 0.89 to 2.3 mg/m^3 ($K(490)$ = 0.1–0.3 m^{-1}). The winter monsoons peak between January and February as the winds blow off the Asian continent and are not conducive to coastal upwelling. Without the forcing mechanism, the regional sea surface temperatures are warmer and temperatures increase along the coast. Correspondingly, chlorophyll decreases when nutrients supplied by upwelling decrease.

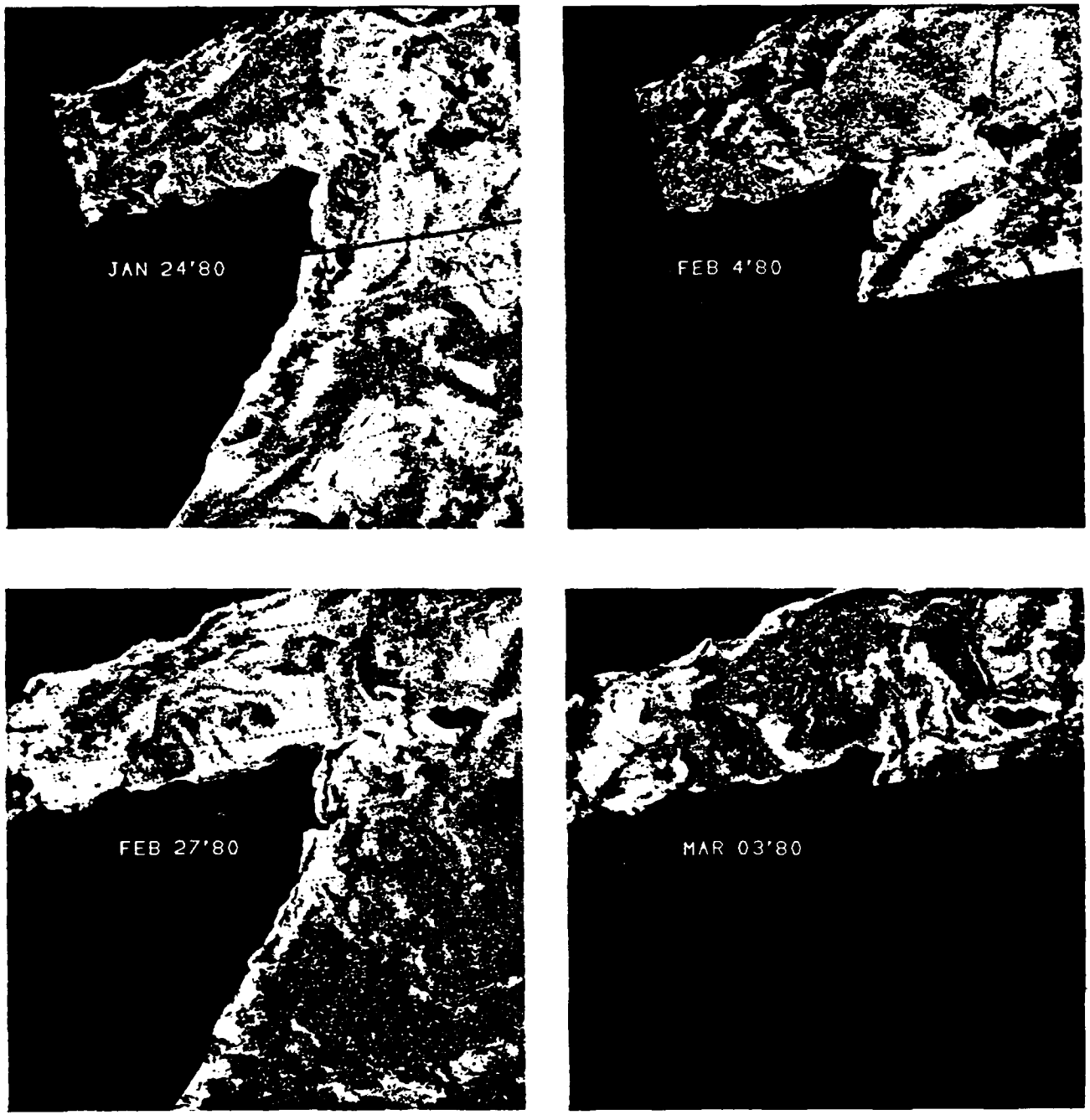

Figure 15. January 24'80, February 4'80, February 27'80, and March 3'80 image sequence.

March 21'80, April 27'80, May 20'80, and June 6'80

In these images (Fig. 16), the Somali current extends northward along the Somali coast into the Gulf of Aden. The chlorophyll levels east of the Somali current are very low (oligotrophic waters). (For this sequence, the low-chlorophyll values are possibly the result of the high E coefficients used in processing, coupled with a consistently lower aerosol radiance value for this four-image sequence relative to the other 36 images processed for this study; see Table 2). At this time, the summer monsoon season is starting. A distinct but narrow flow along the eastern Somali coast gives some early indications that upwelling may be occurring, and the winds shift to a more southwest-northeast flow.

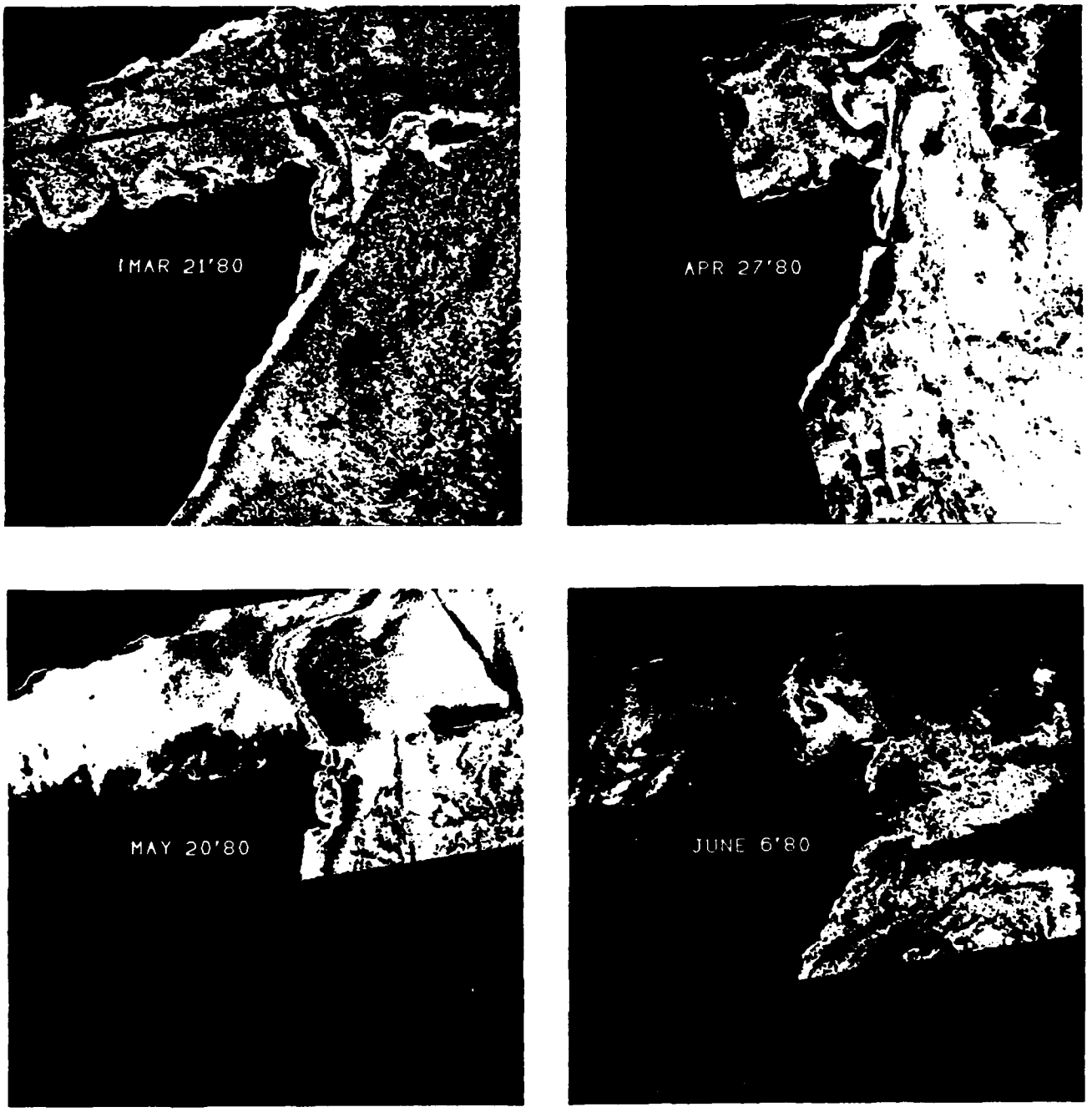

Figure 16. March 21'80, April 27'80, May 20'80, and June 6'80 image sequence.

June 10'80, August 5'80, and August 27'80

This image (Fig. 17) sequence is dominated by intense cloud cover. However, breaks in clouds indicate that chlorophyll concentrations are comparatively normal for this time of year. Levels along the coast are 1.445–2.884 mg/m^3 ($K(490)$ = 0.2–0.4 m^{-1}), and decrease offshore to 0.344–1.445 mg/m^3 ($K(490)$ = 0.1–0.2 m^{-1}). During the summer months, sea surface temperatures in the Gulf of Aden are high (28.9°C), indicating an oxygen-high and nutrient-poor water mass. The chlorophyll levels near 0.042 and 0.080 mg/m^3 ($K(490)$ = 0.025–0.029 m^{-1}) are indicated in the August 5, 1980 CZCS scene.

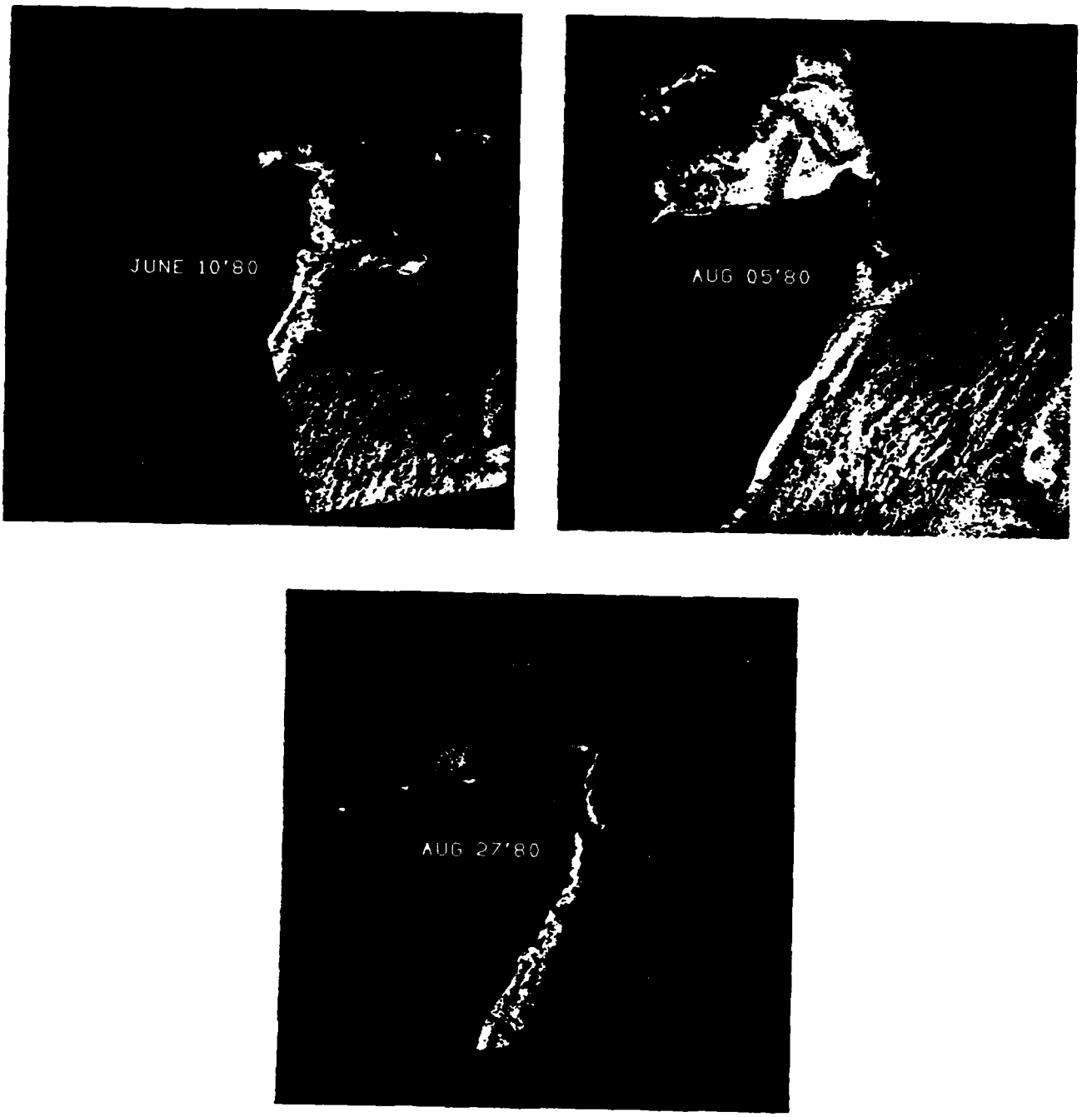

Figure 17. June 10'80, August 5'80, and August 27'80 image sequence

September 20'80—January 27'81

The September 20 and November 7 images (Figs. 18 and 19) show the eastward extension of the Somali current as a wedged region that contains elevated chlorophyll concentrations. The characteristics of the wedge change during this time, however, as the southwestern propagation between 10°N and 9°N is evident.

An anticyclonic eddy (75 km in diameter) of low chlorophyll (*CHL* = 0.042–0.098 mg/m^3; *K*(490) = 0.025–0.031 m^{-1}) is observed in the Gulf of Aden. A similar feature was seen during the same period in the 1979 imagery. Chlorophyll patches occur to the south of Socotra, where concentrations range between 0.38 and 2.5 mg/m^3 (*K*(490) = 0.1–0.4 m^{-1}). The November 7 image shows elevated chlorophyll at the entrance to the Gulf of Aden along the north Somali coast.

The December and January imagery show the same pattern evident in the November 7 image. Additionally, the coastal waters south of Socotra Island indicate a region of high chlorophyll (*CHL* = 2.88 mg/m^3; *K*(490) = 0.4 m^{-1}) that results from upwelling along the coast in response to the onset of the winter monsoon.

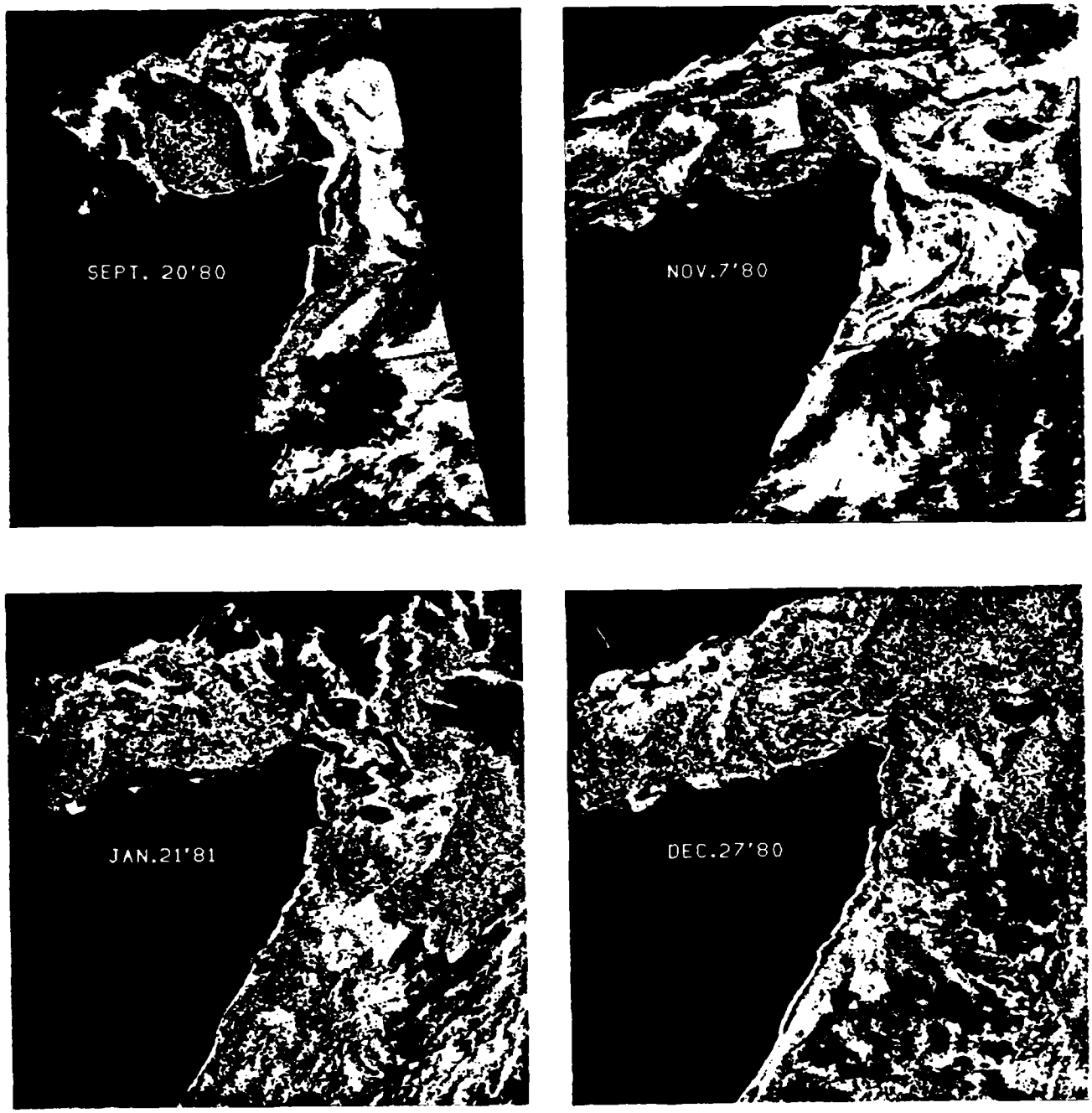

Figure 18. September 20'80, November 7'80, January 21'81, and December 27'80 image sequence.

Figure 19. January 27'81 image.

IV. Conclusions

The variability of ocean optical properties has been described using satellite ocean color data. The complex procedures used in eliminating the significantly high contribution of the atmosphere have been outlined.

Results of a study of CZCS imagery taken along the northeast Somali coast and the Gulf of Aden have been used to generate a full-resolution (1 km) regional image atlas of chlorophyll and optical properties.

This atlas demonstrates the application of the CZCS to provide selected regional optical properties. The results obtained appear reasonable for this area and agree favorably with other investigations of the oceanographic and meteorologic climate. The variability of the optical properties is clearly coupled with physical oceanographic and meteorological forcing. Clearly, the high variability of coastal optical properties requires CZCS imagery to determine the optical climate.

This atlas describes the type of high-resolution data bases that can be developed using satellite data, specifically, remotely sensed ocean color data. The processing and analysis techniques should be applied to ocean color data sets in other regions. Regional optical atlases should be used to plan bathymetric surveys using the Airborne Bathymetric System, and should be included in planning other Navy operations that require an assessment of regional optical parameters. Sea surface temperature distributions and meteorological analyses and forecasts used in conjunction with optical data from regional optics atlases will significantly enhance the Navy's operational understanding of the oceanic environment during unit deployments.

Presently, regional optical data bases can be developed from CZCS imagery to describe the ocean climatology. As future ocean color satellite systems become operational to derive ocean color data, the Navy can easily upgrade any existing CZCS climatology data bases with new optical data. Using the processing and analysis techniques described in this report, the integration of new data sets can be accomplished with a minimum effort. With ocean color remote sensing platforms in the planning stage, such as SeaWifs, the Navy must develop a comfortable expertise with the existing CZCS optical data to make optimum use of future optical data. The development of regional optical atlases and data bases using CZCS data provides the Navy with the opportunity to develop the expertise to use systems planned for the near future.

V. References

Arnone, R. A. (1983). *Secchi Disk Atlas of World Coastlines.* Naval Ocean Research and Development Activity, Stennis Space Center, Mississippi, NORDA Report 83.

Arnone, R. A. and R. A. Oriol (1985). *CZCS Atlas of Water Optical Properties in the Alboran Sea.* Naval Ocean Research and Development Activity, Stennis Space Center, Mississippi, NORDA Report 117.

Austin, R. W. and T. J. Petzold (1980). The determination of the diffuse attenuation coefficient of sea water using the coastal zone color scanner. In: *Oceanography from Space*, J. F. R. Gower, (ed.).

Deutsches Hydrographisches Institute (1960). Monatskarten Fur den Indischen Ozean. Publ. 2422, Hamburg.

Evans, R. (1987). *RSMAS Processing of CZCS Data, Documentation Manual.* University of Miami.

Evans, R. H. and O. B. Brown (1981). Propagation of thermal fronts in the Somali current system. *Deep Sea Research*, 28a:521-527.

Gordon, H. R., D .K. Clark, J. W. Brown, R. H. Brown, R. H. Evans, and W. W. Broenkow (1983). Phytoplankton pigment concentration in the middle Atlantic bight: Comparison of ship determinations and CZCS estimates. *Applied Optics* 22:20-36.

Gordon, H. R. and D. K. Clark (1980). Atmospheric effects in the remote sensing of phytoplankton pigments. *Boundary-Layer Meteorology* 18:300-313.

Gordon, H. R. and D. K. Clark (1981). Clear water radiances for atmospheric correction of CZCS imagery. *Applied Optics* 20:4175-4180.

La Violette, P. E. and T. R. Frontenac (1967). *Temperature, Salinity, and Density of the World's Seas: Arabian Sea, Persian Gulf and Red Sea.* Naval Oceanographic Office, Stennis Space Center, Mississippi, Informal Report 67-49.

Schott, R. (1983). Monsoon response of the Somali Coast and associated upwelling. In: *Physical Oceanography*, Vol. 12, pg. 357-381, Pergamon Press, Ltd.

Distribution List

Asst Secretary of the Navy
Research, Engineering & Systems
Navy Department
Washington DC 20350-2000

Chief of Naval Operations
Navy Department
Washington DC 20350-2000
Attn: OP-71
OP-987

Oceanographer of the Navy
Chief of Naval Operations
U.S. Naval Observatory
34th & Mass Ave., NW
Washington DC 20390-1800
Attn: OP-96
OP-96B

Commander
Naval Air Development Center
Warminster PA 18974-5000

Commanding Officer
Naval Coastal Systems Center
Panama City FL 32407-5000

Commander
Space & Naval Warfare Sys Com
Washington DC 20363-5100

Commanding Officer
Naval Environmental Prediction
Research Facility
Monterey CA 93943-5006

Commander
Naval Facilities Eng Command HQ
200 Stovall St.
Alexandria VA 22332-2300

Naval Oceanographic & Atmospheric
Research Laboratory
Stennis Space Center MS 39529-5004
Attn: Code 100
Code 105
Code 110
Code 115
Code 125L (10)
Code 125P
Code 200
Code 300
Code 321, A. Pressman
Code 330, K. Ferer
Code 350, M. Harris
Code 400
OP-096, D. Montgomery
OP-096, R. Winokur

Naval Oceanographic & Atmospheric
Research Laboratory
Liaison Office
Crystal Plaza #5, Room 802
Arlington VA 22202-5000
Attn: B. Farquhar

Commanding Officer
Naval Research Laboratory
Washington DC 20375

Commander
Naval Oceanography Command
Stennis Space Center MS 39529

Commanding Officer
Fleet Numerical Oceanography Center
Monterey CA 93943-5005

Commanding Officer
Naval Oceanographic Office
Stennis Space Center MS 39529
Attn: R. Caviness
E. Beason
B. Christensan

Commander
Naval Ocean Systems Center
San Diego CA 92152-5000

Commanding Officer
ONR Branch Office
Box 39
FPO New York NY 09510-0700

Commander
David W. Taylor Naval Research Center
Bethesda MD 20084-5000

Commander
Naval Surface Weapons Center
Dahlgren VA 22448-5000

Commander
Naval Underwater Systems Center
Newport RI 02841-5047

Superintendent
Naval Postgraduate School
Monterey CA 93943

Director of Navy Laboratories
Crystal Plaza #5, Room 1062
Department of the Navy
Washington DC 20360

Officer in Charge
New London Laboratory
Naval Underwater Systems Center
New London CT 06320

National Ocean Data Center
1825 Connecticut Ave., NW
Universal Bldg. South, Rm. 406
Washington DC 20235
Attn: G. Withee

Director
Woods Hole Oceanographic Inst
P.O. Box 32
Woods Hole MA 02543

University of California
Scripps Institution of Oceanography
P.O. Box 6049
San Diego CA 92106

Naval Surface Warfare Center
White Oak
10901 New Hampshire Ave.
Silver Spring MD 20904-5000
Attn: Commander
Library

Commanding Officer
Fleet Antisub Warfare Tng Ctr-Atl
Naval Station
Norfolk VA 23511-6495

Defense Mapping Agency Sys Cen
12100 Sunset Hill Rd. #200
Reston VA 22090-3207
Attn: SGWN
Director

Office of Naval Technology
800 N. Quincy St.
Arlington VA 22217-5000
Attn: Code 234, C. Votaw
Code 228, M. Briscoe

Office of Naval Research
800 N. Quincy St.
Arlington VA 22217-5000
Attn: Code 112, E. Hartwig
Code 10D/10P, E. Silva
Code 12
Code 10
T. Kinder, Coastal Sciences
C. Mobley, Coastal Sciences

Commander
Naval Sea Systems Command HQ
Washington DC 20362-5101

Commanding Officer
Naval Civil Engineering Laboratory
Port Hueneme CA 93043

Commander
Naval Air Systems Command HQ
Washington DC 20361-0001

Pennsylvania State University
Applied Research Laboratory
P.O. Box 30
State College PA 16801

University of Texas at Austin
Applied Research Laboratories
P.O. Box 8029
Austin TX 78713-8029

Johns Hopkins University
Applied Physics Laboratory
Johns Hopkins Rd.
Laurel MD 20707

University of Washington
Applied Physics Laboratory
1013 Northeast 40th St.
Seattle WA 98105

D. Wiesenburg
GERGE
10 S. Graham Rd.
College Station TX 77840

Dr. C. McClain
Code 720
NASA/GSFC
Greenbelt MD 20770

Dr. F. Hoge/R. Swift
NASA/GSFC
Wallops Island VA

James L. Mueller
Center for Hydro-Optics and
Remote Sensing
San Diego State University
San Diego CA 92182

Dr. Richard Crout/Dr. Marshall Bradley
Planning Systems, Inc.
115 Christian Lane
Slidell LA 70458

Dr. Robert Evans
Rosenstell School for Marine and
Atmospheric Science
4600 Rickenbacker Causeway
Miami FL 33149

REPORT DOCUMENTATION PAGE

Form Approved
OMB No. 0704-0188

1. Agency Use Only *(Leave blank).*	2. Report Date.	3. Report Type and Dates Covered.
	April 1990	Final

4. Title and Subtitle.

Seasonal Optical Properties Derived from Coastal Zone Color Scanner Satellite Data Along the Somali Coast and the Gulf of Aden

5. Funding Numbers.

Program Element No.	63704N
Project No.	01987
Task No.	300
Accession No.	DN258031

6. Author(s).

Ramon A. Oriol* and Robert A. Arnone

7. Performing Organization Name(s) and Address(es).

Ocean Science Directorate
Naval Ocean Research and Development Activity
Stennis Space Center, Mississippi 39529-5004

8. Performing Organization Report Number.

NORDA Report 244

9. Sponsoring/Monitoring Agency Name(s) and Address(es).

10. Sponsoring/Monitoring Agency Report Number.

11. Supplementary Notes.

*Planning Systems, Inc., Slidell, Louisiana 70458

12a. Distribution/Availability Statement.

Approved for public release; distribution is unlimited. Naval Ocean Research and Development Activity, Stennis Space Center, Mississippi 39529-5004.

12b. Distribution Code.

13. Abstract *(Maximum 200 words).*

Optical water properties of the world's oceans can be obtained from data collected with the Coastal Zone Color Scanner (CZCS) aboard Nimbus-7. Our understanding of the spatial and temporal variability of surface optical properties is greatly improved from synoptic images from visible channel satellites. Current satellite data processing techniques can eliminate the atmospheric contamination that contributes 90% of the visible channel signal. The remaining signal, which constitutes the ocean color, is directly related to the diffuse attenuation coefficient (K) at 490 nanometers for the upper surface waters. Calculation and geographic registration of K can be performed on each 825 m^2 image-pixel of the CZCS data, and results show that the accuracy is within 92% of ship measurements.

Regional coastal optical atlases are required for planning bathymetric surveys using the Airborne Bathymetric System. CZCS data provide a method of deriving temporal and spatial variability of coastal optical properties in regions where limited ship measurements are available. This report presents a demonstration of the capability of a regional optics data base generated using CZCS data.

A series of CZCS images of the eastern Somali coast and the Gulf of Aden has been processed for the diffuse attenuation coefficient and have been used to define a regional optical database. This data base exists in digital image form and clearly defines optical variability in response to continental winds, monsoon winds, and coastal upwelling.

This report represents an initial effort toward generating a regional atlas and demonstrates the methodology to process CZCS data for producing an optical atlas. The procedures for processing, the time requirements, the data handling, and the image file processing are presently being refined and improved based on the procedures used in this regional atlas. This atlas is the initial product produced for the Coastal Optics Planner and is intended as a subset to a global product being generated. Future regional atlases will be produced by the Naval Oceanographic Office in a manner similar to the method shown here.

14. Subject Terms.

ocean color, ocean optics, satellites, multispectral, image processing.

15. Number of Pages.

35

16. Price Code.

17. Security Classification of Report.	18. Security Classification of This Page.	19. Security Classification of Abstract.	20. Limitation of Abstract.
Unclassified	Unclassified	Unclassified	None